Edited by

Horia-Nicolai Teodorescu
Abraham Kandel
Lakhmi C. Jain

FUZZY and NEURO-FUZZY SYSTEMS in MEDICINE

Library of Congress Cataloging-in-Publication Data

Fuzzy and neuro-fuzzy systems in medicine / H.N. Teodorescu, A. Kandel, L.C. Jain, editors.
p. cm. -- (International series on computational intelligence)
Includes bibliographical references and index.
ISBN 0-8493-9806-1 (alk. paper)
1. Fuzzy systems in medicine. 2. Neural networks (Neurobiology)
I. Teodorescu, Horia-Nicolai. II. Kandel, Abraham. III. Jain, L. C. IV. Series.
R859.7.F89F89 1998
610'.285'63—dc21 98-36332
CIP

This book contains information obtained from authentic and highly regarded sources. Reprinted material is quoted with permission, and sources are indicated. A wide variety of references are listed. Reasonable efforts have been made to publish reliable data and information, but the author and the publisher cannot assume responsibility for the validity of all materials or for the consequences of their use.

Neither this book nor any part may be reproduced or transmitted in any form or by any means, electronic or mechanical, including photocopying, microfilming, and recording, or by any information storage or retrieval system, without prior permission in writing from the publisher.

All rights reserved. Authorization to photocopy items for internal or personal use, or the personal or internal use of specific clients, may be granted by CRC Press LLC, provided that $.50 per page photocopied is paid directly to Copyright Clearance Center, 222 Rosewood Drive, Danvers, MA 01923 USA. The fee code for users of the Transactional Reporting Service is ISBN 0-8493-9806-1/98/$0.00+$.50. The fee is subject to change without notice. For organizations that have been granted a photocopy license by the CCC, a separate system of payment has been arranged.

The consent of CRC Press LLC does not extend to copying for general distribution, for promotion, for creating new works, or for resale. Specific permission must be obtained in writing from CRC Press LLC for such copying.

Direct all inquiries to CRC Press LLC, 2000 Corporate Blvd., N.W., Boca Raton, Florida 33431.

Trademark Notice: Product or corporate names may be trademarks or registered trademarks, and are only used for identification and explanation, without intent to infringe.

© 1999 by CRC Press LLC

No claim to original U.S. Government works
International Standard Book Number 0-8493-9806-1
Library of Congress Card Number 98-36332
Printed in the United States of America 1 2 3 4 5 6 7 8 9 0
Printed on acid-free paper

Chapter 4

Contouring Blood Pool Myocardial Gated SPECT Images with Use of a Sequence of Three Techniques Based on Wavelets, Neural Networks and Fuzzy Logic

Luis Patino, André Constantinesco, Ernest Hirsch

1. Introduction

Medical imaging makes currently use of a wide range of non-invasive modalities such as Magnetic Resonance Imaging (MRI), Ultrasound, Computerized Tomography, Nuclear Imaging and Radiography. Although each acquisition modality has its specific application domain, a common point relates all of them. Out of the images acquired, the medical specialists have to recognize a given pathology after adequate presentation or processing of the data. However, due to various reasons (acquisition conditions, distortion, noise, attenuation of the signal, etc.), the images contain only variable amounts of approximated or sometimes incomplete information. In such situations, as a solution to these shortages, fuzzy logic [1], which permits to deal with inaccurate or ill-defined data, is often applied in many areas in the field of medical imaging. Accordingly, over the last years, an increasing number of applications using this approach have been reported in the literature. For example, Boegl et al. [2] have constructed a Computer-assisted on-line diagnosis system, based on fuzzy reasoning, in order to detect rheumatic diseases in radiological images. The assessment of the age of bones based on features automatically extracted from hand radiographs is another example in the field [3]. Other applications of the use of fuzzy logic and reasoning can be found for diagnosing chronic liver diseases in liver scintiscans; see, e.g. Shiomi S. et al. [4]. Further, in the domain of MRI, image segmentation in order to achieve tissue differentiation is described in several publications [5], [6]. The measure of the volumes of cerebrospinal fluid, white and gray matter in brain images (see, as an example, [7]) is also frequently investigated. Lastly, Bezdek published recently a very interesting survey paper showing the currently employed fuzzy methods in medical imaging [8] and, in particular, the increasingly well known fuzzy c-means clustering method is explained.

Use of Neural Networks [9] has appeared in the latest 70's to be an excellent complementary method to fuzzy logic based approaches. Since the parameters used to build a fuzzy system have usually to be tuned heuristically, neural networks, by applying their self-learning capability, can provide a valuable help in the determination of the values of these parameters. Indeed, several contributions combining the two methods for evaluating medical images have been reported. For instance, Lin et al. have used the fuzzy set theory combined with a convolution neural network for reducing the detection of false-positives in digital chest radiographs [10]. So-called Neuro-Fuzzy techniques have been developed for tissue classification in MRI data [11].

The chapter is devoted to the description of the development of an alternative automated method to extract the contours of the left ventricle in blood pool Single Photon Emission Computed Tomography (SPECT) images. The method combines wavelets theory, neural networks and fuzzy logic to build a complete procedure for the extraction of contours to be used for computing the Left Ventricle Ejection Fraction (LVEF). The outline of the contribution is as follows. Section II describes briefly how the kind of images we work with are obtained and how the information they encode has to be interpreted. The overall strategy of the method we suggest for processing the image sets in order to determine the LVEF is introduced in section III composed of five parts. The three parts following the introduction summarize the aim of the techniques combined into a single system. These are a wavelets based pre-processing of the data, a segmentation into regions of interest using neural network approaches and a recognition technique built around fuzzy logic components. The section ends with the description of the parallel learning procedure we have developed and implemented in order to train the system and fix automatically its parameters. Representative results obtained with our method are given in section IV for both validating experiments making use of specifically built phantoms and clinical test cases based on real patient data. Section V concludes our contribution and gives a short outlook.

2. Anatomy of the G-SPECT images

Blood pool myocardial Gated Single Photon Emission Computed Tomography (G-SPECT) images are acquired in our laboratory with an Elscint Helix gamma camera equipped with a low-energy, high-resolution collimator. After radiolabeling the red blood cells with technetium 99m, a set of 30 electrocardiographic (EGC) gated projections of 40 sec with 8 phases of the cardiac cycle is obtained when rotating the camera 180° from the right anterior oblique position to the left posterior oblique position, the patient being in supine position. Each projection image is corrected for non-uniformity and the center of rotation is also adjusted. After filtered backprojection using a Butterworth filter with a cut-off frequency of 0.35, three kind of heart axis reoriented slices are obtained: Horizontal Short Axis (HSA), Horizontal Long Axis (HLA), and Vertical Long Axis (VLA) images as shown in Figure 1. Each of these sets of slices of 1.2 cm thickness is further divided for this work into a Diastolic Subset and a Systolic Subset.

The most informative set from the three available data sets is the HSA images set. The main reason for this is that this latter set can be meaningfully used to calculate the

Left Ventricle Ejection Fraction (LVEF). This ratio is defined as the difference between the diastolic and systolic heart volumes, divided by the diastolic heart volume. It is now well known that the left ventricle ejection fraction is one of the most useful parameter describing the cardiac function. A normal value of the left ventricle ejection fraction should lie in the range 59%-65%.

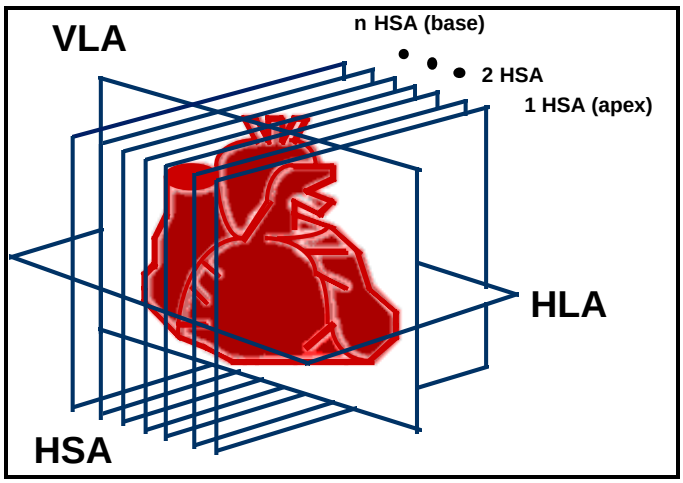

Figure 1. Schematic representation of the different acquired image sets after application of a backprojection algorithm.

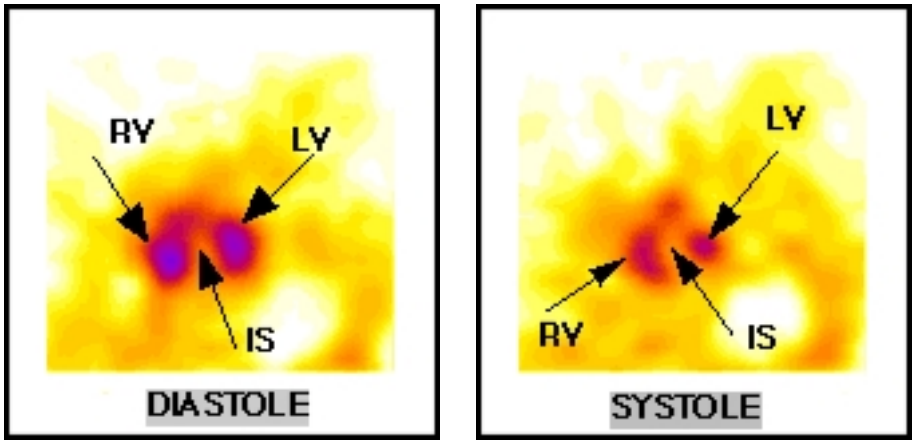

Figure 2. Typical HSA images from the same midventricular slice with Left Ventricle (LV), Right Ventricle (RV), Interventricular Septum (IS) and residual radiation, showing the diastolic and systolic phases of the cardiac cycle.

In our case, the main parts to recognize are the left and right ventricles, the inter-ventricular septum, the atriums and the valve planes. In addition, due to the specific acquisition and backprojection processes used, a residual radiation contours the whole

myocardium (see Figure 2). Further, for the first or two first images in the HSA set, it can happen that only the heart in its diastolic phase can be seen. This can be understood if one recalls that the ventricular volume is greater in this phase and that the apical motion of the left ventricle is important. On the other hand, in the last HSA images, usually only the atriums can be seen and no longer the right and left ventricles (see Figure 3). Thus, for the whole set of images, the actual location of the ventricles in the different images must be established. Conventionally, the last image to be evaluated is the one in which the left ventricle appears and is recognized because its area is approximately the same in the diastolic and the systolic phases, corresponding to the mitral valve plane.

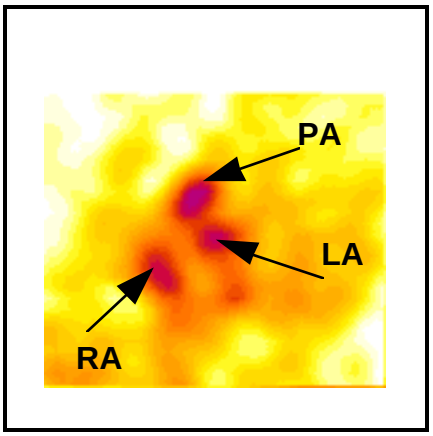

Figure 3. Example of an HSA image at the base of the heart showing the atriums: Right Atrium (RA), Left Atrium (LA) and the Pulmonary Artery (PA).

One of the major problems in analysis of blood pool myocardial scintigraphy image data is to separate accurately the right and left ventricles. As experimentally evidenced, when the septum is too thin, the gamma diffusion radiation coming from the adjacent ventricles superpose each other, giving the effect of having in the images one unique uniform region including the right ventricle, the left ventricle and the septum. In most of these cases, the expert observer corrects the images manually by erasing the right ventricle and closing the contour of the left ventricle. A second problem encountered when trying to establish precisely the frontiers of the ventricles is the noise introduced in the acquired data during both the acquisition and the reconstruction processes. This leads to blurred boundaries, which disable separating the two ventricles. A further important problem is related to the automated left ventricle recognition. This pattern recognition problem has a high degree of complexity due to the great variety of observed heart forms, which can strongly vary according to the characteristics of a patient and of his pathology. Only one fully automated recognition procedure for this task has been reported in the literature [12] using myocardial instead of volume blood pool images. However, some semi-automated methods have been also proposed (see, e. g., [13]).

3. STRATEGY OF THE PROPOSED METHOD

3.1. Overview of the method

The proposed algorithm consists in the application of three processing steps executed sequentially. The first operation carried out is a wavelet-based pre-processing [14], [15] which has in charge to remove as much noise as possible from the images, to separate the two ventricles when these organs form a single uniform region and to determine approximately the border of the left ventricle image region. The second procedure applied achieves the segmentation of the images and is performed using a neural network implementing the ART (Adaptive Resonance Theory) algorithm [16-18]. Lastly, application of a neuro-fuzzy system enables the recognition of the left ventricle and of its contour. For this latter step, an off-line learning process step is required to create the rule base allowing reasoning with the neuro-fuzzy system.

3.2. Wavelets-Based Image Pre-Processing

Wavelets are a mathematical tool enabling the decomposition of a signal according to different resolutions. Their great advantage is their ability to analyze a signal with the same accuracy in both the time and frequency domains. This is not the case when applying Fourier analysis where the accuracy is favored either in the frequency domain or in the temporal domain. In other words, increasing the accuracy in one domain implies a decrease in precision in the other domain. Further, wavelets are also known for their capacity to identify singularities associated with fine variations of the signal to be evaluated (the image intensity in our case) [19], [20]. Lastly, wavelets provide also an inherent smoothing property due to the fact that noise can be filtered out at low resolutions. The difficulty at this stage of the image analysis is thus to choose the appropriate resolution at which the images should be analyzed, in order to achieve the best compromise between noise reduction and extraction power of singularities. The multiresolution scheme proposed by Mallat [21] is a possible candidate for solving this difficulty and enables to extract the signal singularities and to reduce noise at high frequencies. Going from one resolution to the next finer resolution is achieved through doubling the band frequency of the filters associated with the two resolutions, as a result of the underlying sampling operations. Other authors, see for example Nguyen [22], firstly analyzed the frequency response of the family of filters to be used and then derived a multiresolution analysis scheme by changing the sampling rates of the filters, allowing this way the analysis of different bands of frequencies. In our method, we propose to analyze the images with two different high pass filters defining two frequency bands.

In our implementation, we have chosen to use the first and second derivatives of a Gaussian function as the wavelet functions. The coefficients of the filters are obtained after having sampled both functions at a frequency of 0.5 $pixel^{-1}$. The resulting frequency bands are respectively 0.06-0.22 $pixel^{-1}$ for the filter corresponding to the first derivative of the Gaussian function and 0.04-0.16 $pixel^{-1}$ for the one associated with the second derivative of the Gaussian function. The second derivative based filter

is applied first in order to enhance the gray-level variations between the endocardium and the septum. As a result, the second derivative of the Gaussian function leads to a filter, also known as the Mexican hat filter [15], which has one central positive peak and a negative lobe on each side of this peak. This particular form enables, while applying the filter by convolution, to correct the filtered values in order to decrease the adjacent values of the central point of convolution. Consequently, in the images and particularly in the septal regions, this allows to reduce the image intensities influenced by the nuclear emissions coming from the adjacent heart cavities.

In a second step, the filter based on the first derivative of the Gaussian function is applied to detect the contour points. This filter avoids false detections, as it is well known that detection of local maxima of the resulting gradient is more optimal than extracting the zero crossings of the second derivative [19,20]. Further, an averaging low pass filter with constant coefficients of value 0.4 is used to smooth the image after application of each high pass filter.

The filters are applied as suggested by Mallat. Firstly, all the image lines are processed and secondly the columns. After each filtering step, the low pass filter is applied in a direction orthogonal to the high pass filter used.

Choosing the appropriate resolution at which the images should be analyzed is a function of both the intrinsic resolution of the acquisition system and of the level of detail to be detected in the images. After evaluation of a rather exhaustif set of images, taking the acquisition conditions into account, the frequency characteristics of the filters could be defined as indicated above. Accordingly, the wavelets coefficients have been derived enabling to process optimally the images obtained in our laboratory. Even though our algorithm has been specifically tailored to be suited to our acquisition system, it can also work with other systems, the design of the filters being related mostly to resolution and not to the internal parameters of the camera (in our case, a gamma camera).

3.3. Neural Network Based Image Segmentation

Neural networks, aimed at trying to emulate biological neural networks [9], are known as non-linear cognitive systems able to store and to learn new models which can then be used for subsequent pattern recognition or classification operations. Neural networks are usually implemented as parallel structures performing the often large amount of computations implied. Further, a wide variety of neural network architectures can be found in the literature. The implementation proposed and developed by Carpenter and Grossberg [16], [17] is one among the most known and is particularly suited for classification tasks. Their algorithm works as follows. Assuming no a priori knowledge about the different classes to be defined during the process and for each element in an initial set of data to be classified, the neural network performs a first classification operation according to a similarity measure. For that purpose, one element in the set is chosen as the representative of a first class and designated as its leading element or leader. Then, if another element from the initial set can be considered similar to this leader, it is classified in the corresponding class. If this element fails to be similar enough, it is used as the leader of a new class. After treatment by the neural network of all the elements, the result obtained is a set of

leaders each representing a class defined by the elements fulfilling the similarity criterion associated with the corresponding leader.

In our application, for segmenting the pre-processed images, we have chosen to implement a neural network similar to the structure proposed by Carpenter and Grossberg. As a result, each class defined after completion of the processing is associated with a specific region in the image, the area corresponding to the first initial class being defined as the region corresponding to the left ventricle. Further, the dimensional characteristics of each region depend strongly on the gray level value of the pixel chosen as the leader of the initial class. Accordingly, if the leader of the first class is chosen randomly, there is no usable criterion available enabling to certify that the dimensions of the corresponding region are indeed those of the left ventricle. In order to improve the accuracy of these measures, we have chosen to initialize the classification step using the image intensity value of a given pixel previously extracted by the wavelet-based filtering step. This pixel is defined in our case as the contour point being located in the image on the boundary between the region corresponding to the left endocardium and the area associated with the septum. This choice enables to define the gray level value of the initial class to be used as the starting point for the neural network based classification and segmentation step.

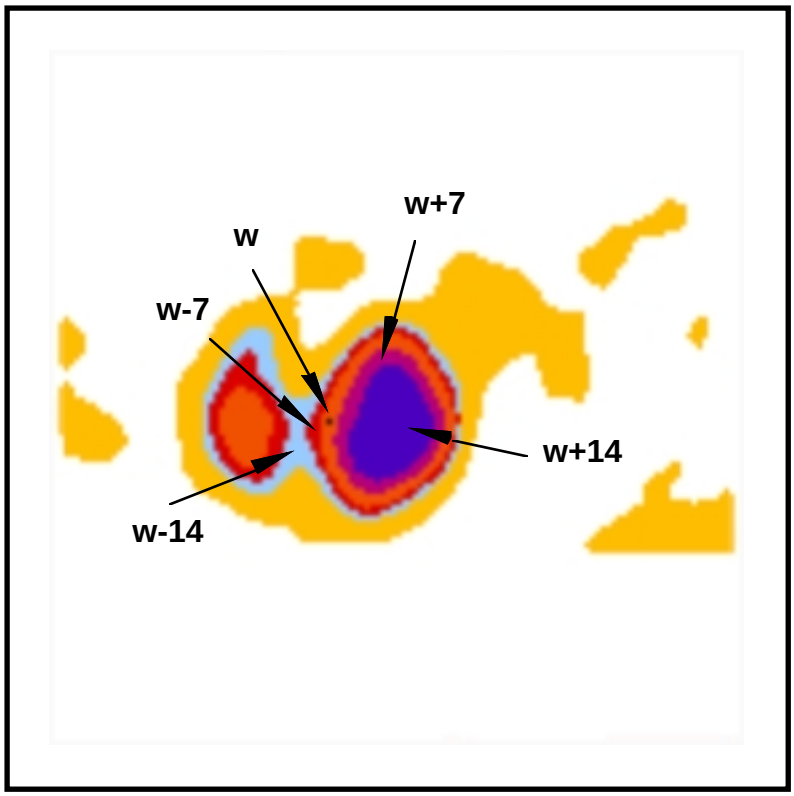

Figure 4. Typical resulting segmented image (zoom: x2) after neural network based processing (the corresponding input HSA diastolic slice is given in Figure 2).

Our implementation of the neural network has been achieved using two layers, the first layer being the so-called input or comparison layer and the second one being the output or classification layer. Each layer itself is composed of five neurons whose transfer functions are defined as Gaussian functions. The third of these five Gaussian functions has its central value located at the gray level value w given by the specific contour point output by the wavelets based processing step. The other central peak values are then defined respectively through displacements by multiples of seven. The central values of the Gaussian functions are thus placed, as follows, at *w*-14, *w*-7, *w*, *w*+7, *w*+14. (The value 7 has been chosen heuristically to achieve a good segmentation resolution around *w*). This way to proceed allows to establish guidelines in order to segment the image and classify its contents, without establishing the total number of classes and their centers in advance. This approach for classification is referred to as "partially supervised classification" [23]. The neural network based segmentation method developed has the advantage to need no operator intervention to initialize the ART procedure. Further, the implementation is also rather straightforward. Even though both initial class and gray level resolution are important parameters of the segmentation task and control the quality of the results, it has to be recalled that the initial leaders (acting as some kind of seed points) correspond to meaningful points delivered by the wavelet based extraction procedure. Implementation of other methods, such as the so-called k-means approach, would require more effort without providing results of better quality. The same comment holds for the completely supervised k nearest neighbours method. In comparison to more standard region segmentation techniques (such as, e. g., region growing or split and merge approaches), our approach has the valuable major advantage to deliver results of comparable quality in much shorter times, as there are, strictly speaking, no iterations to execute. A typical segmentation result, corresponding to the HSA diastole slice shown in Figure 2, appears in Figure 4.

3.4. Fuzzy logic based recognition of the regions of interest (ventricles)

3.4.1. Definition of the required fuzzy sentences

One of the most difficult steps in medical image evaluation systems trying to recognize automatically organs, such as ventricles in G-SPECT images, is to differentiate the organ of interest, in our case the left ventricle, from the other organs represented in the image such as vessels, etc. As a matter of fact, for our specific application, even in the cases where just the right and left ventricles are visible in the images, it is hard to establish without any ambiguity which of the two is the left ventricle. This is in particular due to changes, from one patient to the other or even from one image slice to the other for a given patient, in both position and form of the ventricle.

In order to associate at the best a given region in the images with the left ventricle, we can assume that its cavity should be contained within the limits defined in the image by two concentric segmented regions of respectively minimal and maximal size, defining some kind of dimensional tolerances for the imaged ventricle. The output of

the neural network based segmentation process delivers regions of nearly the same gray level value those borders are defined by some sort of level lines in the original gray value images. Each of these regions is a tentative candidate for being recognized as the left ventricle. If we take separately each of these level lines, as illustrated in Figure 4 above, for determining the corresponding enclosed region and its association with the myocardium, several hypotheses may be generated for relating the left ventricle to a segmented region. In Figure 5, we show the different associations that can be issued after a typical image segmentation step. We call this series of images exploded images. The first image at the top left will be immediately discarded because of its shape and dimensions and the choice will take place between the four remaining images.

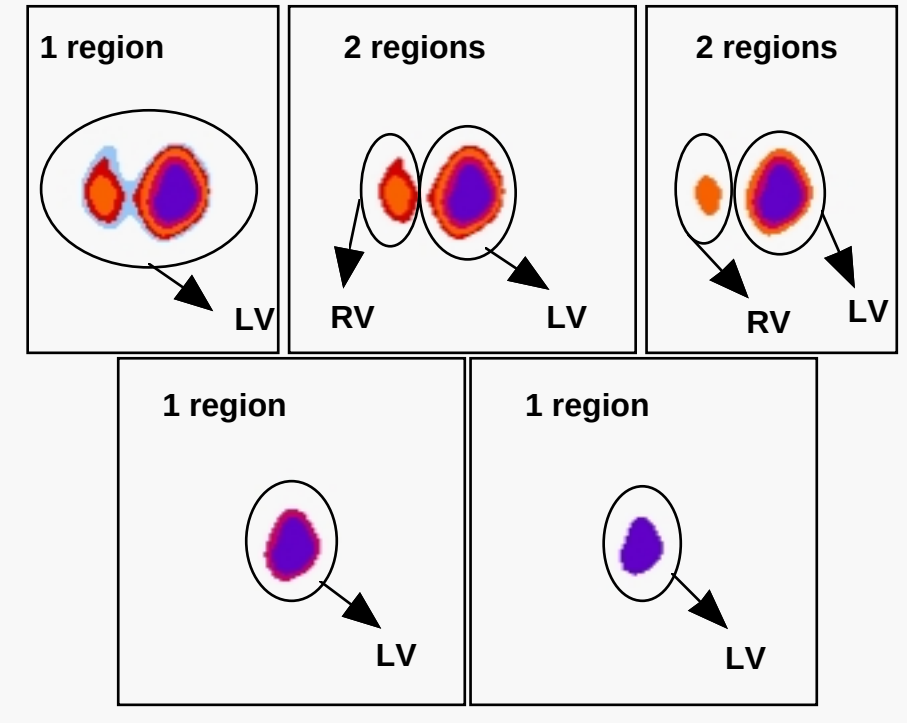

Figure 5. Left ventricle - region association hypotheses after a typical segmentation step (the input image is given in Figure 4.).

In order to allow later the automated recognition of the region to be considered as the left ventricle, each region is described with a series of measured geometric parameter values. These measures, considered as the most descriptive for the image contents taking our final goal into account, are the following:

- *Number of slices in the image set*. This enables us to determine which region of the myocardium (in the direction of the short axis) is currently being analyzed. This region usually is either the apex, the base of the heart or the area in between. For the three types of regions, both the shape and the dimensions of the myocardium

may vary quite largely.

- *Number of regions in the image*. This value can be helpful for locating the left ventricle in the images and for defining accurately its borders with the atriums. As demonstrated experimentally, when we recognize the apex of the myocardium in the image, then we surely have only one region in the image, which is the left ventricle with a high degree of confidence. Going ahead with this reasoning, when we are in a region corresponding to the middle of the myocardium, then we should encounter two other regions corresponding respectively to the left and right ventricles. Also, near a region corresponding to the base of the heart where the boundaries with the atriums are located, the number of segmented regions should increase to three or even more. Of course, smaller segmented regions produced by arteries and other organs (as the great vessels) can also be observed and make recognition an even more difficult task.
- *Area of a region*. This parameter becomes very meaningful when associated with the left ventricle region. It is on one hand very informative about the growing of the region associated with the left ventricle from the apex to the base, and thus can serve to maintain coherence when assigning sense to the regions in the various slices. Its value can also, on the second hand, be used ultimately to calculate the ejection volume fraction if one recalls that a pixel corresponds in fact to a spatial elementary volume of the organ (i. e. a voxel).
- *Circularity of a region*. This value describes essentially the shape of the left ventricle region in each slice of the set of HSA images to be evaluated. At the beginning of the image sequence, the region corresponding to the apex appears more or less like a circle. Progressing in the sequence, this region progressively takes on an increasingly elliptical form. In our implementation, the circularity value is determined as follows. Firstly, the area and the perimeter of each region are computed. Then, we calculate the two radii corresponding respectively to this area and this perimeter. Lastly, the ratio between these two radii is defined as the desired circularity value (the coefficient being equal to 1 if the region is circular). We have implemented an automated procedure to compute the area and perimeter of each region without operator manipulation, using some basic functions from the public domain NIH image processing software [24].
- *x and y Coordinates of the center of gravity of a region* . These information pieces allow to locate the region under evaluation in the image. It should be noted here that all the evaluation is carried out in the short axis plane.

After having evaluated this parameter set for all the segmented regions present in the set of slices under investigation, we obtain a data structure called *heartinfo*, an example of which is given in Table 1. With the exception of the data of column 2, added here to provide a better understanding of the measures shown, this data structure is the basic input for the following recognition process based on fuzzy logic techniques. The data of the fourth column is normalized in the following way. In the first exploded image of the first slice of the set, the area of the region considered as the left ventricle is taken as a reference. The area of the regions in all the other exploded images (and thus also in the other slices) is divided by this reference value. Thus, a relationship can easily be established between the slices since the resulting normalized coefficient

generaly grow from the first to the last slice. In this sense, the coefficient acts as some kind of inter-slice information. Data in the sixth and seventh columns are normalized with respect to the maximum value found in each column.

To analyze and interpret this data structure, sentences defined using fuzzy logic approaches are applied. Since there is no commonly agreed model available for representing the myocardium in every shade of representation that clinicians might encounter in medical routine, fuzzy logic is used to circumvent this shortage. As a prerequisite, a knowledge base, applicable for the various interpretation contexts encountered when evaluating a sequence of slices and identifying the right values (fixed or in specified sub ranges) for the parameters enabling to recognize the left ventricle among all the segmented regions, has to be devised. This is achieved taking advantage of the fuzzy logic framework, which allows to specify knowledge in the form of a set of rules expressed in a way comparable to every day speaking. These rules will constitute the inference engine based on the well-known *modus ponens* law summarized below:

Implication : **IF** fuzzy_antecedent **THEN** fuzzy_consequence
Premise : `fuzzy_antecedent` **has** `degree_of_truth`
Conclusion : `consequence` **has** `certainty_value`

Using this mechanism, we can build rules following the model given in the example below:

IF `Area_of_the_region is Big` **THEN** `Region is The_left_ventricle`

`Area_of _the_region` and `Region` are antecedent variables. `Big` and `The_left_ventricle` are fuzzy antecedent and consequent sets respectively. When fuzzy sets are constituted with one constant element it is called a singleton. In our application, `The_left_ventricle` would be a singleton.

Table 1. Example of measures summarized in the data structure *heartinfo*. The parameters correspond to the regions obtained after segmentation of a set of five HSA slices. The fifth slice corresponds to the image given Figure 4.

Slice number	Exploded image	Number of Regions	Area of possible LV	Circularity of possible LV	x Position of possible LV (pixels)	y Position of possible LV (pixels)
1.0000	1	1	1.0000	1.8066	0.7143	0
1.0000	2	1	0.3613	1.9333	0.7143	-0.2000
1.0000	3	1	0.2514	1.9450	0.7143	-0.2000
2.0000	1	1	0.7948	1.8963	0.7143	-0.1000
2.0000	2	1	0.4306	1.9669	0.7143	-0.2000
2.0000	3	1	0.3006	1.9541	0.5714	-0.2000
3.0000	1	1	0.9480	1.8883	0.5714	0.1000
3.0000	2	1	0.4249	1.9536	0.5714	-0.1000
3.0000	3	1	0.2659	2.0001	0.5714	-0.1000
3.0000	4	1	0.1474	2.0253	0.5714	-0.2000
4.0000	1	2	2.0318	1.8612	0.5714	0.3000

4.0000	2	2	1.6936	1.8860	0.4286	0.3000
4.0000	3	2	1.4017	1.8588	0.4286	0.3000
4.0000	4	2	1.1705	1.8530	0.4286	0.3000
4.0000	5	2	0.7081	1.8192	0.4286	0.2000
5.0000	1	1	2.3555	1.9094	0.5714	0.2000
5.0000	2	2	2.0058	1.8866	0.4286	0.3000
5.0000	3	2	1.6792	1.9201	0.4286	0.3000
5.0000	4	1	1.3671	1.9036	0.4286	0.3000
5.0000	5	1	0.8873	1.8541	0.2857	0.3000

Combination of all the measured parameters encoded in *heartinfo* into one consistent rule enables to define a sure and powerful tool to discriminate image data. In our application, the measured parameters have been combined as follows:

IF
`Number_of_slice_in_the_image_set` is `Member_of_the_first_acquired_images`
and `Number_of_particles_in_the_image is Small`
and `Area_of_the_region is Big`
and `Circularity_of_the_region is High`
and `x_Coordinate_of_the_region is Well_horizontally_centered`
and `y_Coordinate_of_the_region is Well_vertically_centered`
THEN
`Region is The_left_ventricle`

In the rule above, new fuzzy sets, such as `Small`, `Big`, `Member_of_the_first_acquired_images`, `High`, `Well_horizontally_centered` and `Well_vertically_centered`, have been introduced. In fact, fuzzy logic makes no assumption, nor defines rules, on how many fuzzy sets must be established in order to determine meaningfully the value of a fuzzy variable. In the same way, the membership functions describing how to manipulate the fuzzy sets may take on various user-defined forms. The Gaussian, triangular and trapezoidal membership functions are among the most popular and commonly used functions.

An experienced user can greatly take advantage of this freedom in defining the membership function shapes and in choosing the number of fuzzy sets, allowing him to set or to modify the fuzzy system according to its accumulated experience when applying the system on real data.

In earlier contributions, we have heuristically established the number of fuzzy sets and the parameters (coefficients) of the membership functions [25], [26]. Although the corresponding implementations were able to deliver rather good results when evaluating real-life G-SPECT image sequences, sensible application required a long time to correctly and manually tune the system parameters. Further, a clear disadvantage is also that this parameter value fixing procedure must be carried out again every time the knowledge base has to be up-dated, because either new rules are added or new membership functions are devised. To overcome this limitation and to make the implementation more versatile, we have recently developed a new module that automatically creates rules and membership functions, based on evaluated image sequences of patients being diagnosed. Using this learning set of data, the knowledge base is computed by this new module using an approach mixing the so-called neural

network ART algorithm and the fuzzy system FUNNY [27]. The automated determination of the knowledge base and the associated learning phase will be detailed in Section 3.5.

3.4.2. Combining neuronal approaches and fuzzy logic based inference systems

Neural networks can contribute decisive and important advantages to the efficiency of use of fuzzy logic based systems. Among other interesting features of neural networks, the ability to carry out the computations in parallel, the possibility to model a function and the invaluable learning capacity can be mentioned. Accordingly, so-called neuro-fuzzy systems have recently been reported in the literature, based on various types of learning processes. These approaches can tentatively be classified as follows, according to the learning mechanism they use :

- Learning capacity enabling to define new membership functions for the manipulation of the fuzzy sets. However, the rule base is defined once for all a priori and thus cannot be changed.
- Learning capacity, enabling to define new rules. However, this time, the membership functions are considered specified once for all a priori and thus remain constant.
- Learning capacity enabling to adapt in "real time" (that is during execution of the application) the parameters defining the membership functions.
- Learning capacity enabling to change in "real time" the weights of the rules in the rule base.

Several approaches combining the learning capacities defined above have been proposed. For example, Berenji and Khedkar [28], [29] have suggested a system based on what they call "reinforcement learning algorithm". The approach consists in evaluating the actual and next possible states of the system based on the history of the already undertaken actions. The evaluation results then are used to determine or modify the membership functions, implementing this way the learning capacity. The same learning behavior can be achieved using the FUNNY (FUzzY or Neural Net) system developed by Bersini and Gorrini [27]. This latter system is based on the gradient based learning method, firstly described by Nomura, Hayashi and Wakami [30]. A comparable approach is used in the ANFIS (Adaptive Neuro-Fuzzy Inference System) method proposed by Jang [31], [36]. Other contributions go a step further and suggest approaches providing not only a learning capacity for the membership functions, but also a possibility to change dynamically the dimension of the rule base. The work of Sulzberger et al. [32] and of Nauck and Kruse [33], [34] are representative examples of this way to proceed.

Most of the implemented systems including a learning capacity for the membership functions are designed using the so-called Sugeno fuzzy model [30], [35]. Sugeno fuzzy rules are characterized by the fact that rules have to be written according to the template indicated below:

$$\textbf{\textit{IF}}\ x \text{ is } A \text{ and } y \text{ is } B\ \ \textbf{\textit{THEN}}\ \ z = f(x,y)$$

In the rule template above, x and y are antecedent variables, A and B are from fuzzy antecedent sets and $z = f(x,y)$ is a so-called crisp function in the consequent part of the

rule. The function *f* is a polynomial in *x* and *y* and the order of the polynomial crisp function determines the order of the resulting Sugeno fuzzy system. The most widely used systems are first order Sugeno System. The Sugeno system of order zero is identical to the system described above where the consequent part of the rule is expressed as a singleton.

Jang in his work has built an equivalent to the Sugeno first order inference system using neural networks. In this approach, the following two Sugeno fuzzy rules *R1* and *R2* find their equivalent in Jang' ANFIS system as indicated in Figure 6.

R1 : ***IF*** *x is A1 and y is B1* ***THEN*** *z1 = f1(x,y)*
R2 : ***IF*** *x is A2 and y is B2* ***THEN*** *z2 = f2(x,y)*

Jang has further suggested to differentiate the nodes in the neural network, in order to use a part of them as adaptive nodes for which the parameters may be changed and to use the other part as fixed nodes having no parameters and those functions are thus fixed. The former type of nodes is usually graphically represented by squares while the latter type is shown as circles in the figure below.

The first layer or input layer of the neural network structure suggested by Jang has in charge to evaluate the set of premises of the antecedent parts in the fuzzy implications defined for our system. To achieve this, each input premise is evaluated by the node in the first layer associated with a fuzzy set. Thus, each of these nodes acts as an adaptive node and has as transfer function the membership function defining the associated fuzzy set. The set of parameters defining the different membership functions in this layer is the set of the corresponding premise parameters. The second layer is constituted by fixed nodes defined each by the fuzzy function "and". The algebraic product or the computation of the minimum between two numbers are the most popular operators used for implementing the "and" functions. The value output by each node of the second layer represents the so-called fired strength of the associated rule. The task of the nodes in the third layer is only to normalize the set of fired strengths. This is achieved using a fixed node, which simply computes the ratio between the fired strength of its corresponding rule and the sum of the fired strength of all the rules manipulated by the system. The fourth layer is again an adaptive layer, the nodes of which are evaluating functions of the type $z = f(x,y)$ which represent the consequent parts of Sugeno fuzzy rules as described previously. These functions take as input the normalized fired strengths delivered by the third layer. The parameters defining the polynomial functions are the so-called consequent parameters. The last layer or output layer of the neural neural is built using a fixed node which simply computes the sum of all the consequents parts output by layer four.

In our implementation, we followed a similar approach, the inference system being slightly different in comparison to the ANFIS system. In Figure 7, we give the graphical representation of our system, making use of the ANFIS graphical convention.

We have also decided to combine the three last layers of the neural structure described above into one layer acting, thus, as output layer. This layer, placed at the end of the network, uses a fixed node whose transfer function is the so-called max operation associated. The reason for our choice is that, considering our applied goal, we only want to use rules enabling to recognize the left ventricle. In our implementation,

on one hand, if a region in a given image does not correspond to the ventricle, then, when applied to the input of the neuro-fuzzy recognition system, it will simply lead to fire no rule.

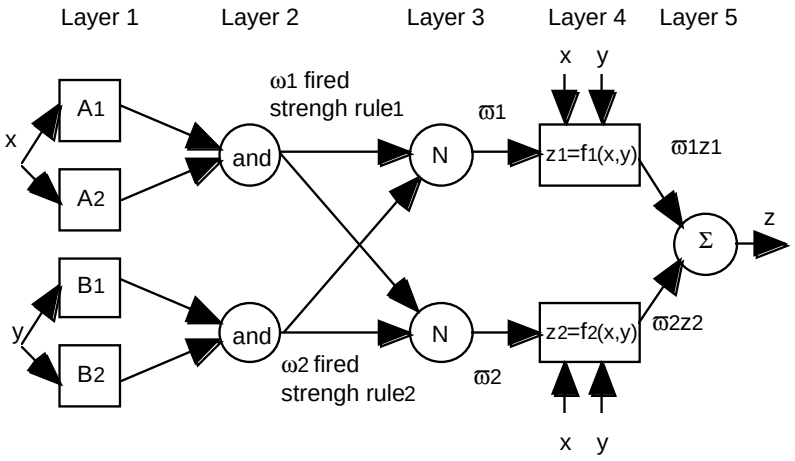

Figure 6. Equivalent ANFIS rule for a two input first order Sugeno fuzzy model with two rules (after J.-S. R. Jang in [35b]).

On the other hand, we need still several rules describing the various situations in which the left ventricle has to be recognized. Accordingly, when a region corresponding actually to the left ventricle is input to the system, then the neural network will fire one or several rules of the rule base, the others being not fired as they correspond to outputs associated with the recognition of "another kind of left ventricle" which, possibly, is greater, or more circular, etc. We have thus established a series of rules placed in a rule base and describing the left ventricle. The region under evaluation will be recognized as such if its parameters fulfil at the best one of the rules in this rule base. Therefore, in that way we take as output of the network the maximum strength of the fired rule.

In our case, the membership functions defining the fuzzy sets for the premises to be used in the nodes of the first layer are isosceles triangular functions, the parameters of which are determined during the training (learning) phase of the recognition system. During the same learning process, the number of membership functions corresponding to each input and the number of corresponding rules are also determined.

In order to exemplify how recognition of the left ventricle in an image is achieved, let us take as input to be analyzed the image shown on Figure 1. The first steps of our recognition procedure consists in applying to the image the wavelets based pre-processing algorithm and the neural network based segmentation operation. The result of these operations has already been shown on Figure 3. Next, the resulting image is "exploded", that is the various tentative interpretations are determined, as represented in Figure 4. In the resulting set of exploded images, the parameters of the region they contain are evaluated and these data are stored in a table as depicted in Table 1. This

data structure is the input data for the subsequent recognition processing steps.

We can now apply the developed neuro-fuzzy logic system schematically represented in Figure 7. The membership functions and the rule base have been defined during the training of the system using data of three patients. As already described, the system works with triangularly shaped membership functions for the input nodes.

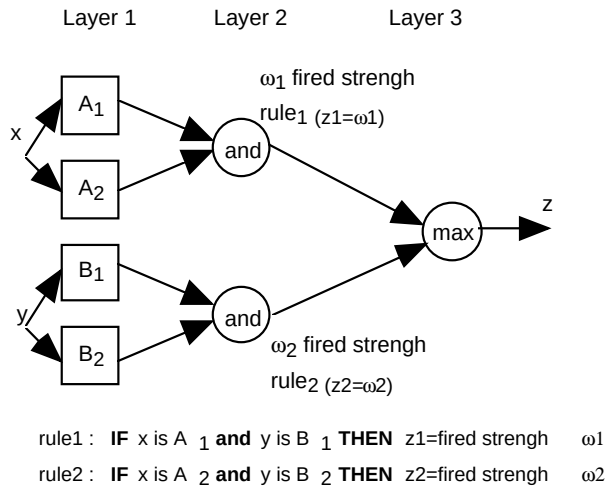

Figure 7. Graphical representation of the equivalent neural network inference system implemented.

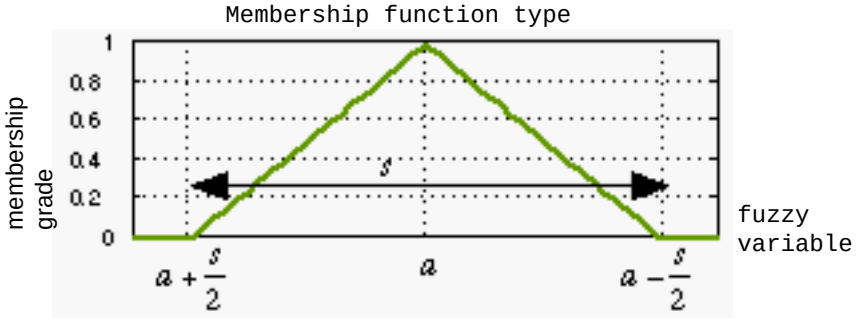

Figure 8. Shape and parameters of the triangular membership functions used.

These symmetric functions are characterized by their center *a* and their support *s*, as shown on Figure 8. The whole set of membership functions is represented in Figure 9, each line shown representing the membership function corresponding to an input parameter of the first layer.

The rule base itself contains 62 rules. But, owing to simplicity in the presentation of our example, we give as representative samples only the six rules likely to be fired during the processing. This is shown using a matrix representation in the Table 2.

Table 2. Matrix representation summarizing the parameters of the six rules able to be fired

	fuzzy set associated with variable1 with mf	fuzzy set associated with variable2 with mf	fuzzy set associated with variable3 with mf	fuzzy set associated with variable4 with mf	fuzzy set associated with variable5 with mf	fuzzy set associated with variable6 with mf
rule 1	mf11	mf21	mf31	mf43	mf51	mf61
rule 2	mf12	mf21	mf33	mf41	mf51	mf61
rule 3	mf13	mf21	mf33	mf41	mf51	mf61
rule 4	mf13	mf21	mf35	mf42	mf51	mf62
rule 5	mf14	mf22	mf37	mf41	mf52	mf62
rule 6	mf15	mf22	mf34	mf41	mf52	mf62

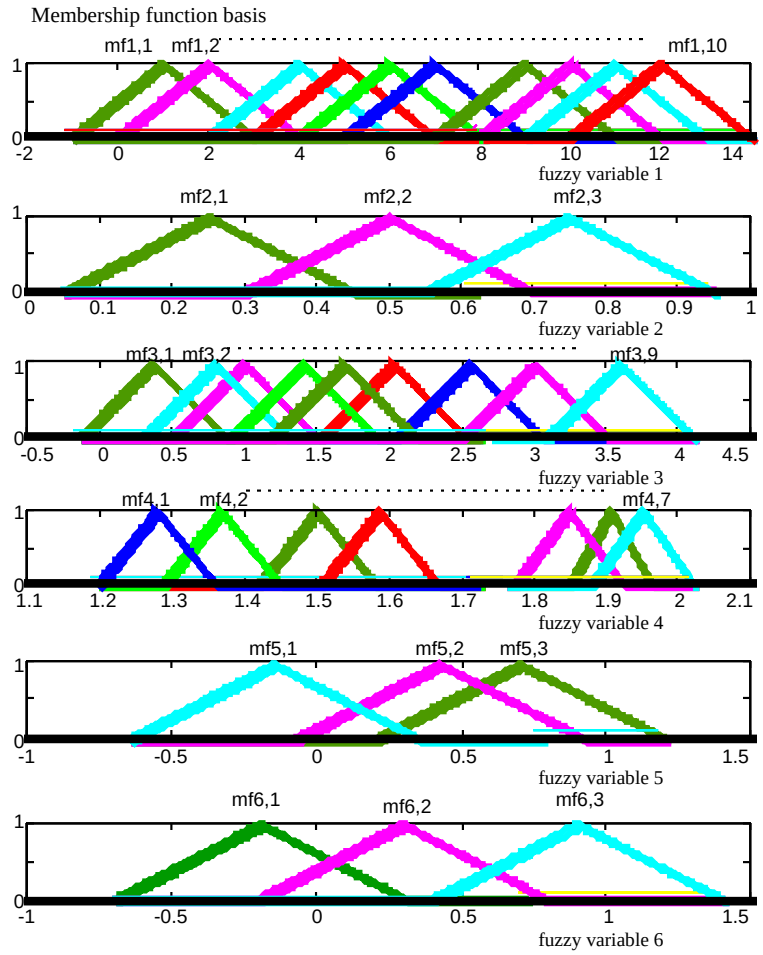

Figure 9. Whole set of membership functions implemented in the first layer of the neuro-fuzzy recognition system

The (compact) representation above can be interpreted in the following way for rule 1:

IF `parameter1` is `The_fuzzy_set_associated_to_variable1_with_mf11`
and `parameter2` is `The_fuzzy_set_associated_to_variable2_with_mf21`
and `parameter3` is `The_fuzzy_set_associated_to_variable3_with_mf31`
and `parameter4` is `The_fuzzy_set_associated_to_variable4_with_mf41`
and `parameter5` is `The_fuzzy_set_associated_to_variable5_with_mf51`
and `parameter6` is `The_fuzzy_set_associated_to_variable6_with_mf61`
THEN `left_ventricle is the fired strengh of the rule.`

After evaluation of the image data by the system, we obtain as results the fired strengths of the rules used and their associations with the corresponding regions. The

max operator is then applied to each processed image to choose the region approaching at best the description of the left ventricle encoded in the rules. In Table 3, the computed fired strengths are given, together with the selected region representing the left ventricle (shaded zone). In Figure 10 below, this same selected region is shown in a square. The other left ventricle hypothesis for the remaining exploded images are shown circled.

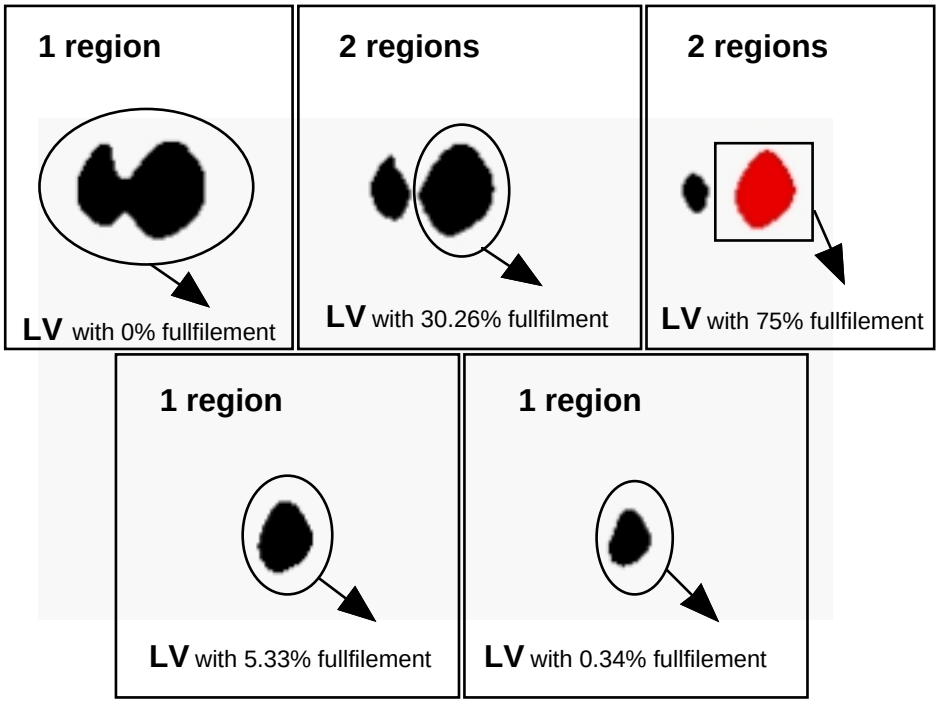

Figure 10. Selected regions in each exploded image resulting from partitioning an actual input image (see also Figure 5). The region representative of the left ventricle is shown in a square.

This result then allows us to firstly isolate the right region and secondly to extract automatically the contours of this area which will lastly describe the left ventricle. This is achieved knowing the gray level value of the finally selected region and its location. Lastly, a so-called zigzag search algorithm is applied to the region retained in order to contour the whole region. The algorithm is executed until all the perimeter points have been collected. The principle of this final operation and its result are shown in Figure 11.

Table 3. Fired strengths computed and selected representative for the left ventricle (results correspond to the example given in section 4.1 Table 1 and Figure 5).

Slice	Explode	fired	fired	fired	fired	fired	fired
5.0000	1	0	0	0	0	0	0
5.0000	2	0	0	0	0	0.2241	0.3026
5.0000	3	0	0	0	0	0.7507	0.1137
5.0000	4	0	0	0.0533	0.0524	0	0
5.0000	5	0	0	0.0034	0	0	0

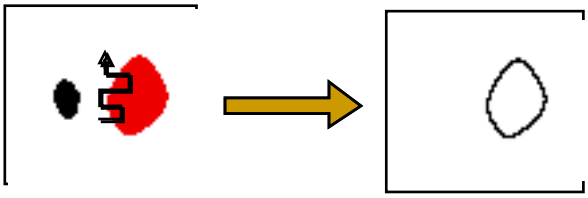

Figure 11. Principle of the final processing step (zigzag search algorithm) and its result.

As a conclusion to this section, a typical example of the final results obtained for a whole set of diastolic and systolic images of a patient is showed in Figure 12.

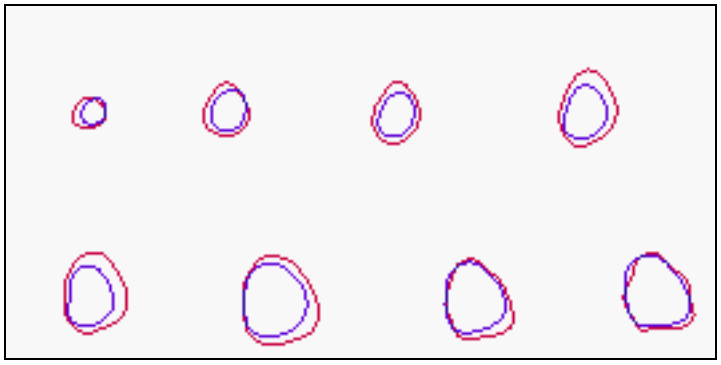

Figure 12. Typical final results for a full set of images of a patient. Diastolic contours are the outer ones, Systolic contours are the inner ones.

3.5. Training the recognition system using a neuro-fuzzy technique

The purpose of training the recognition system is twofold as explained earlier. First, it allows to create and to determine the parameters of the membership functions to be associated with the fuzzy sets used to evaluate each of the input measurements. Second, it enables to set up the rule base encoding the knowledge necessary to perform the recognition of the left ventricle. We have set as a requirement for the system to be

developed that these tasks should be carried out automatically, that is without operator intervention. This makes on one hand the system comfortable to use. If it is considered necessary to enlarge the knowledge base to improve its recognition ability or to correct some particular rules, there is no waste of time in order to tune the system. On the other hand, this enables to deal with a knowledge base containing a relative large number of rules and membership functions, a task that may not be easy for a human operator. We can meet our requirement through the parallel combination of two methods. These are the so-called ART leadership algorithm described in section 3.3., also used during the image segmentation step, and a neuro-fuzzy learning approach inspired from the "FUNNY" system developed by Bersini and Gorrini [27]. In fact, use of the ART based approach is sufficient to satisfy our requirements. We have however chosen to add the neuro-fuzzy learning mechanism in order to be able to cope with situations for which classification is poor or wrong, even though the necessary rules and membership functions are available. In this fashion, we are able to optimize somewhat the system implemented.

3.5.1. Automated generation of rules and membership functions (ALGORAM)

In this section, we introduce a new approach for automatically producing the membership functions and rules to be stored in the knowledge base. This method makes use of ALGORAM, an acronym for "Automatic Leader Generation Of Rules And Membership functions ." The method has been devised following a procedure similar to that used for the design of the leadership algorithm described in section 3.3. We have chosen to partially label the data, as we have decided to select several leaders from the input set. It has to be recalled that the groups forming the initial partition of the data are known a priori. We then select a leader in each group and arrange them into a vector that is said to be labeled.

In order to get a better understanding of the method proposed, consider again the data shown in Table 1 summarizing the parameters corresponding to the regions obtained after segmentation of a typical input image and for which we want to build the necessary membership functions and a rule base to be used in a further recognition and interpretation step of the region corresponding actually to the left ventricle. Recall that each raw in this table corresponds to a so-called "exploded" image extracted from a given slice in the whole image set to be evaluated. For example, there are four "exploded" images for the first, second and third slices and five "exploded" images for the fifth slice. Each slice can thus be considered to constitute a group of partitioned images. For each slice, or equivalently the associated group of partitioned images, the operator of the system designates manually a leader in order to start the training phase, pre-labeling the regions of interest. This leader is naturally chosen as being the segmented region, which can be considered to correspond at best to the left ventricle. If the selection of these initial leaders is badly performed, the training system will need more iterations to learn to recognize (and reject) regions which exhibit only weak coherence among themselves. As a consequence, the system then generates supplementary membership functions for each input variable to avoid misclassification.

This results in a decrease of execution speed and can be, in some extreme cases, the cause of mistakes when evaluating other patients.

Table 4. Expansion of Table 1 in order to include labels for the exploded images in each slice corresponding at best to the left ventricle

Slice	Particles	Area	Circularity	x Position	y Position	Label
1.0000	0.2500	1.0000	1.8066	0.7143	0	0
1.0000	0.2500	0.3613	1.9333	0.7143	-0.2000	1
1.0000	0.2500	0.2514	1.9450	0.7143	-0.2000	0
2.0000	0.2500	0.7948	1.8963	0.7143	-0.1000	1
2.0000	0.2500	0.4306	1.9669	0.7143	-0.2000	0
2.0000	0.2500	0.3006	1.9541	0.5714	-0.2000	0
3.0000	0.2500	0.9480	1.8883	0.5714	0.1000	1
3.0000	0.2500	0.4249	1.9536	0.5714	-0.1000	0
3.0000	0.2500	0.2659	2.0001	0.5714	-0.1000	0
3.0000	0.2500	0.1474	2.0253	0.5714	-0.2000	0
4.0000	0.5000	2.0318	1.8612	0.5714	0.3000	0
4.0000	0.5000	1.6936	1.8860	0.4286	0.3000	0
4.0000	0.2500	1.4017	1.8588	0.4286	0.3000	1
4.0000	0.2500	1.1705	1.8530	0.4286	0.3000	0
4.0000	0.2500	0.7081	1.8192	0.4286	0.2000	0
5.0000	0.5000	2.3555	1.9094	0.5714	0.2000	0
5.0000	0.5000	2.0058	1.8866	0.4286	0.3000	0
5.0000	0.5000	1.6792	1.9201	0.4286	0.3000	1
5.0000	0.2500	1.3671	1.9036	0.4286	0.3000	0
5.0000	0.2500	0.8873	1.8541	0.2857	0.3000	0

In the following, we note *x* each of the input regions to be evaluated and tl the partially labeled vector built by grouping together the leaders selected for each slice or partition group. It must however be understood that vector tl will act much more as a set of flags providing links to the leaders required by our algorithm than as the expected value to be returned by the recognition system. For example, for the fourth slice, the fourth exploded image could as well be chosen to represent tentatively the left ventricle. However, in this example, it has been preferred to select the third image of the partition because, in the diastolic phase, the surface of the imaged area is expected to be rather large. However, in the case of a patient with a smaller heart, the input region could better match the fourth region in the fourth slice. It would also make no sense to have the recognition system returning a value of zero. As indicated in section 3.4.2, the only requirement is that the region tentatively associated to the left ventricle leads to a value larger than those of all the other regions in the slice. Indeed, all the candidate regions for representing the left ventricle should be characterized by high values, whereas regions corresponding to the right ventricle, the atriums or great vessels should have small values.

The problem to be solved can now be formalized. For that purpose, let us define the variables and parameters as indicated in the table below:

VARIABLE		DESCRIPTION
X		is the set of input regions which can be recognized as representing the left ventricle (candidate regions)
x_{ij},	i=1,,m j=1,,n	is the collection of m region vectors, each characterized by n parameters
G_k,	k = 1,..., o	are the m partition groups obtained after segmentation, or, in other words, the collection of m slices in a given patient image set
sl_{kj},	k = 1,..., o j = 1,..., n	is the collection of selected leader regions, each characterized by n parameters
f_i,	i = 1,..., m	is the collection of labels acting as flags pointing to the selected leader regions
y_i,	i = 1,..., m	is the collection of the m crisp outputs of the recognition system corresponding respectively to the m input vectors (see section 3.4.2)
rl_{kj},	k = 1,..., o j = 1,..., n	is the collection of returned leaders, each characterized by n parameters
MF		is the set of membership functions
q_j,	j = 1,..., n	is a vector specifying the number of membership functions to be used for each input
mf_{jp},	j = 1,., 3×n p = 1,, q_j	is the collection of membership functions for the recognition system
sg_j,	j = 1,..., n	is a constant vector containing n sigma values to be used as a support to built a given membership function
RU		is the set of rules
ru_{hj},	h = 1,..., r j = 1,..., n	is the collection of r rules characterized by n parameters to be used for recognition

As an example, according to the set of images corresponding to the data collected in Tables 1 and 4, the parameters *m*, *n* and *o* are such that *m* = 22, *n* = 6 and *o* = 5. The values of the parameters *p*, *q* and *r* will be fixed during the training phase as shown later. The training and learning process has now to follow in order the steps below.

- **a. Automated generation of rules and membership functions for the selected leader in the first slice of the image sequence.** We firstly build triangularly shaped membership functions such that their parameters fulfil the relations $a_{1j} = sl_{1j}$. The support of these functions is given by the sigma vector sg defined in the table above. Choosing small values for sigma for each parameter already leads to an increase of the knowledge base since more membership functions and rules must be used to classify the data. Membership functions are finally stored using the following format:

$m_{1p} = sl_{1j} - sg_j/2,\ j = 1,\ldots,n$ and $p = 1, 4, \ldots, (3\times n) - 2$
$m_{1p} = sl_{1j},\ j = 1,\ldots, n$ and $p = 2, 5, \ldots, (3\times n) - 1$
$m_{1p} = sl_{1j} + sg_j/2,\ j = 1,\ldots,n$ and $p = 3, 6, \ldots, (3\times n)$

Accordingly, the rules matching these membership functions are also created and the vector **q** is also updated. That is :

$ru_{1j} = 1$ and $q_j = 1,\ j = 1,\ldots,\ n$

- **b. Verification step**. This step checks if the leader in the next slice of the image sequence leads to firing. Indeed, it is possible that, in this slice, the region corresponding to the left ventricle has just slightly changed. In this case, it will be recognized using the same rules and membership functions than for the leader in the preceding slice. If the changes are too important, some of the parameters are no longer in agreement with the currently defined membership functions and new functions and rules have to be generated in order to take into account the data which have not led to firing.

- **c. Addition of rules and membership functions for the parameters which have not led to firing.** In most of such situations, in general, only one or two parameters did not led to firing for a newly selected leader. Thus, we have just to add the necessary supplementary information. This avoids rewriting of a whole vector of membership functions and accordingly duplication of effort. Also, the vector q is updated, incrementing component q_j by one unit if j is the index of the input with no firing. The update of the membership functions is slightly different from their automated generation, at shown below :

$m_{q(j)p} = sl_{q(j)j} - sg_{q(j)}/2,$
where j corresponds to data unable to fire and $p = (3\times j) - 2$
$m_{q(j)p} = sl_{q(j)j}$,
where j corresponds to data unable to fire and $p = (3\times j) - 1$
$m_{q(j)p} = sl_{q(j)j} + sg_{q(j)}/2,$
where j corresponds to data unable to fire and $p = (3\times n)$

The corresponding new rules are created based on the existing rules. Even if a rule is not fired, some of its parameters are evaluated. The fired strengths of the rules are thus recalculated, with the difference that in this case the previously used implication operator, the product between numbers, is replaced by the sum between numbers. This enables to select the rule with the greatest fired strength. This rule in turn enables to point to a region with characteristics similar to that of the leader inducing the updates. The rule is simply modified as follows:

$ru_{h+1j} = ru_{1j}\ ,\ j=1,\ldots,\ n$

$ru_{h+1j} = q_j$, where j corresponds to data unable to fire

- **d. Verification of classification quality.** During this step, we verify that the leader returned by the recognition system is the same previously selected leader. The returned leader parameter vector rl_{kj} is obtained as follows:

  $rl_{kj} = x_{uj}$, with $y_u > y_v, , u \bullet v$ and $x_{uj} > x_{vj}, \in G_k$

  In order to assess the similarity between the two parameter vectors, we compute the Euclidean distance between the selected leader parameter vector and the one of the returned leader in the respective partition group G_k :

  $D_k = //sl_{kj} - rl_{kj} //$

  If the distance above is equal to zero, we can proceed with the treatment of the next leader to evaluate and verify the quality of classification. In this case, the two groups G_k and G_{k+1} are combined into a so-called super-group. In order to assign a unique representative region to this super-group, the parameter vector rl_{kj} or rl_{k+1j} leading to the largest fired strength is selected. If the distance is not zero, then the rule base has to be modified and possibly new membership functions added, as described in the next section.

- **e. Addition of rules and eventually of membership functions to avoid misclassification.** It can be taken as granted that the output value of the recognition system for a new leader will not be one. This is due to the fact that, contrary to the case of the leader selected in the very first slice, no new rules, in which each premise is associated with a membership function centered on the value of each parameter characterizing the new leader, have been created. In order to avoid misclassification and to obtain an output value for the new leader larger than the value of any other region in the partition group, the rule with the worst fulfilled premise has to be modified. This is achieved by replacing this premise by a new one with an associated membership function centered on the value of the corresponding leader input parameter.

  If we note ru_h the rule with the highest strength and ru_{hj} the premise j of the rule which is worst fulfilled, we are able to define $J = //sl_{kj} - m_{up}//$ the cost function for partition group *k*, where *j* is the index of the worst fulfilled parameter, $p = (3 \times j)-1$ and $u = 1,.., q_j$. If there exists a value of *u* such that *J* is below a given threshold, then the corresponding rule is modified as follows:

  $ru_{h+1j} = u$, where *j* is the index of the worst fulfilled parameter.

  If no value of u fulfills the threshold condition, the rule has to be associated with a

newly created membership function as follows, after having increased q_j by one unit :

$m_{q(j)p} = sl_{q(j)j} - sg_{q(j)}/2$, where j is the index of the worst fulfilled parameter and $p = (3\times j) - 2$
$m_{q(j)p} = sl_{q(j)j}$, where j is the index of the worst fulfilled parameter and $p = (3\times j) - 1$
$m_{q(j)p} = sl_{q(j)j} + sg_{q(j)}/2$
where j is the index of the worst fulfilled parameter and $p = (3\times n)$
$ru_{h+1j} = q_j$, where j is the index of the worst fulfilled parameter

f. Return to step b. (New iteration of the process)

In Table 5 and Figure 13 below, the operating mode of the training/learning process is exemplified. The numerical values reported correspond to the example already introduced in Table 4.
After evaluation by the neuro-fuzzy inference system, the rules corresponding to a leader which have been fired are hold back. According to the example above, the rules having been fired are the rules 1, 2, 3, 7 and 8. The created corresponding membership functions are shown in Figure 13 in the same order.

3.5.2. Adjustment of membership functions using a descent method (FUNNY)

Nomura, Hayashi and Wakami [30] have proposed an interesting method enabling the fuzzy inference systems to tune by themselves their parameters ("self-tuning") during a learning/training process. This technique is particularly suited for approaches using Sugeno zero order models for implementing the fuzzy logic system. In their contribution, these authors suggest a procedure to correct the parameter values of the membership functions associated to the premises and conclusion of a given rule. The procedure is based on the minimization of a so-called objective function involving the error E between a reference output y^r and the actual output y.

The equation corresponding to a rule of a Sugeno zero order model is remembered below :

IF $x_{1,1}$ is $m_{1,p}$ and $x_{1,2}$ is $m_{2,p}$ and $x_{1,j}$ is $m_{1,p}$ and ... and $x_{1,n}$ is $m_{3*n,p}$
THEN y is b_h for the rule number h.

Table 5. Learning process for the example given in Table 4. Corresponding problems and their solutions as determined automatically by our training process. mf stands for membership function.

Parameter values						Problem to be solved	Solution
mf11	mf21	mf31	mf41	mf51	mf61	START	-
mf12	mf21	mf32	mf41	mf51	mf61	2th image badly Classified! (on 1th Patient data set used)	Addition of 2 mf and 1 rule to avoid misclassification
mf13	mf21	mf32	mf41	mf51	mf62	3th Image badly Classified! (on 1th Patient data set used)	Addition of 2 mf and 1 rule to avoid misclassification
mf13	mf21	mf33	mf41	mf51	mf62	4th Image: no rule fired! 1mf does not exist	Addition of 1 mf and 1 rule
mf14	mf21	mf33	mf41	mf51	mf62	5th Image: no rule fired! 1mf does not exist	Addition of 1 mf and 1 rule
mf14	mf22	mf33	mf41	mf51	mf62	5th Image: no rule fired! 1mf does not exist	Addition of 1 mf and 1 rule
mf15	mf21	mf33	mf42	mf51	mf62	4th Image badly Classified! (on 1th Patient data set used)	Addition of 2 mf and 1 rule to avoid misclassification
mf14	mf22	mf33	mf41	mf52	mf62	5th Image badly Classified! (on 1th Patient data set used)	Addition of 1 mf and 1 rule to avoid misclassification

The error E is given by:

$$E = \frac{1}{2}\left(y - y^r\right)^2$$

If we note a the center of the triangle and s its support, then the learning process, or the adjustment or evolution of the parameters, can be described by the following equations:

$$a_{hj}(t+1) = a_{hj}(t) - k_a \frac{\partial(E)}{\partial a_{hj}}$$

$$s_{hj}(t+1) = s_{hj}(t) - k_s \frac{\partial(E)}{\partial s_{hj}}$$

$$b_h(t+1) = b_h(t) - k_b \frac{\partial(E)}{\partial b_h}$$

where k_a, k_s, k_b are adaptation learning factors and t the number of iterations.

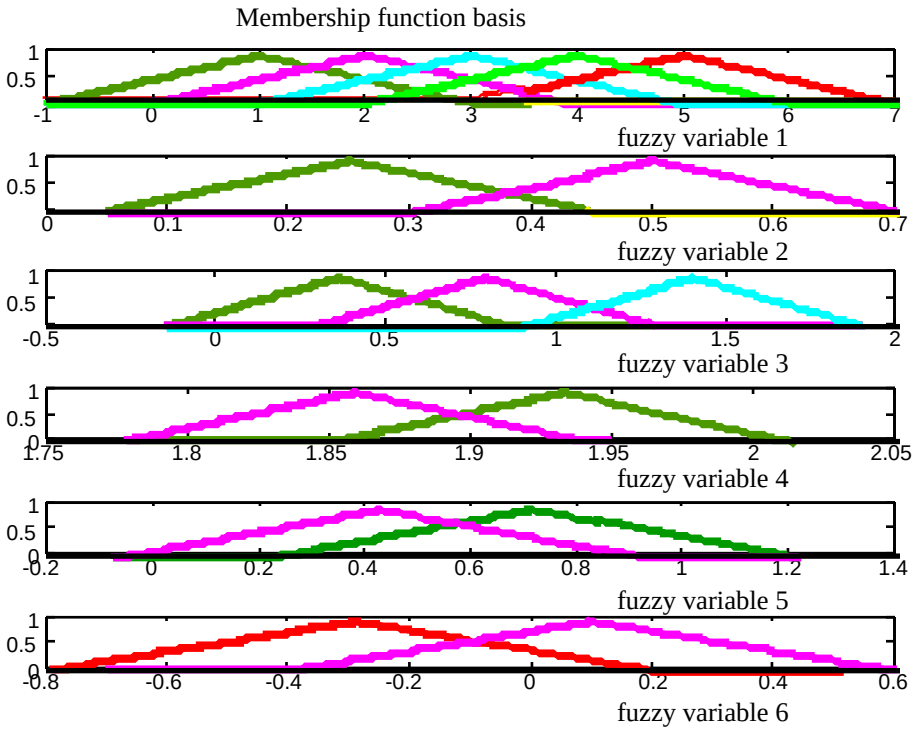

Figure 13. Membership functions created during the training process. They correspond to the example given in Table 4 and to the data summarized in Table 5.

In this method, a given membership function can be adjusted according to the local error E associated with each fuzzy rule and independently to its semantic meaning. This sometimes leads to results which make no sense. An example of the inconsistencies which can occur is given by the membership function associated with the fuzzy set "`small`". After adaptation of this function, it can happen that the associated range of values is larger than those of the fuzzy set "large".

In order to take this drawback into account, Bersini and Gorrini [27] have proposed an improvement of the method. They suggest to link all rules referring to the same membership functions before proceeding with the adjustments, enabling this way to keep the common semantic meaning for all rules. Further, using a gradient-based approach, Bersini and Gorrini propose to express the learning formulas as follows:

$$\frac{\partial(E)}{\partial a_{rj}} = \frac{2k_a\left(y_i^r - y_i\right)\left(\sum_{h=1}^{tmf_{rj}} \omega_h b_h - y_i \sum_{h=1}^{tmf_{rj}} \omega_h\right)\operatorname{sgn}\left(x_{ij} - a_{rj}\right)}{\sum_{h=1}^{tr} \omega_h s_{rj} mf_{rj}\left(x_{ij}\right)}$$

$$\frac{\partial(E)}{\partial s_{rj}} = \frac{k_s\left(y_i^r - y_i\right)\left(\sum_{h=1}^{tmf_{rj}} \omega_h b_h - y\sum_{h=1}^{tmf_{rj}} \omega_h\right)\left(1 - mf_h\left(x_{ij}\right)\right)}{\sum_{h=1}^{tr} \omega_h s_{rj} mf_{rj}\left(x_{ij}\right)}$$

$$\frac{\partial(E)}{\partial b_r} = \frac{k_b \sum_{h=1}^{tb_r} \omega_h \left(y_i^r - y_i\right)}{\sum_{h=1}^{tr} \omega_h}$$

where tmf_{rj} is the total number of rules including `mfrj` in their premises, *tr* the total number of rules, ω_k the fired strength of the `h`th rule and *sgn(x)* the sign of x.

In this approach, since no consequents are defined for a rule as we simply take as output the maximum strength of the rule, we have accordingly slightly modified the learning equations to be used as indicated below:

$$\frac{\partial(E)}{\partial a_{rj}} = \frac{2k_a\left(y_i^r - y_i\right)\left(\sum_{h=1}^{tmf_{rj}} \omega_h^2 - y_i \sum_{h=1}^{tmf_{rj}} \omega_h\right)\mathrm{sgn}\left(x_{ij} - a_{rj}\right)}{\sum_{h=1}^{tr} \omega_h s_{rj} mf_{rj}\left(x_{ij}\right)}$$

$$\frac{\partial(E)}{\partial s_{rj}} = \frac{k_s\left(y_i^r - y_i\right)\left(\sum_{h=1}^{tmf_{rj}} \omega_h^2 - y_i \sum_{h=1}^{tmf_{rj}} \omega_h\right)\left(1 - mf_{rj}\left(x_{ij}\right)\right)}{\sum_{h=1}^{tr} \omega_h s_{rj} mf_{rj}\left(x_{ij}\right)}$$

3.5.3. Combining the automated generation of rules and membership functions and the adjustment of their parameters in a parallel implementation (FUNNY-ALGORAM)

The main objective set for the combination of the two techniques is to achieve an implementation leading to an optimized system. If we always create a membership function every time a piece of data is badly classified or a rule could not lead to firing, the system rule base grows and may become too large. Applying the FUNNY algorithm simultaneously to the ALGORAM Method enables to "push and pull" the membership functions. This allows an input parameter to lead to a larger or smaller value, depending on the modified location of the membership function center after a displacement introduced by the FUNNY algorithm. To achieve this, we have added (by having checked if a leader is well classified) an intermediate step in our procedure ALGORAM as follows:

- a. Create rule and membership function for first leader.
- b. Check if next leader leads to firing.
  - Add rule and membership function for parameters which disabled firing.
- c. Check if leader is well classified.
  - Apply the FUNNY algorithm to optimize all membership functions.
  - If application fails, add rule and possibly membership function to avoid misclassification.
- d. Go to step b.

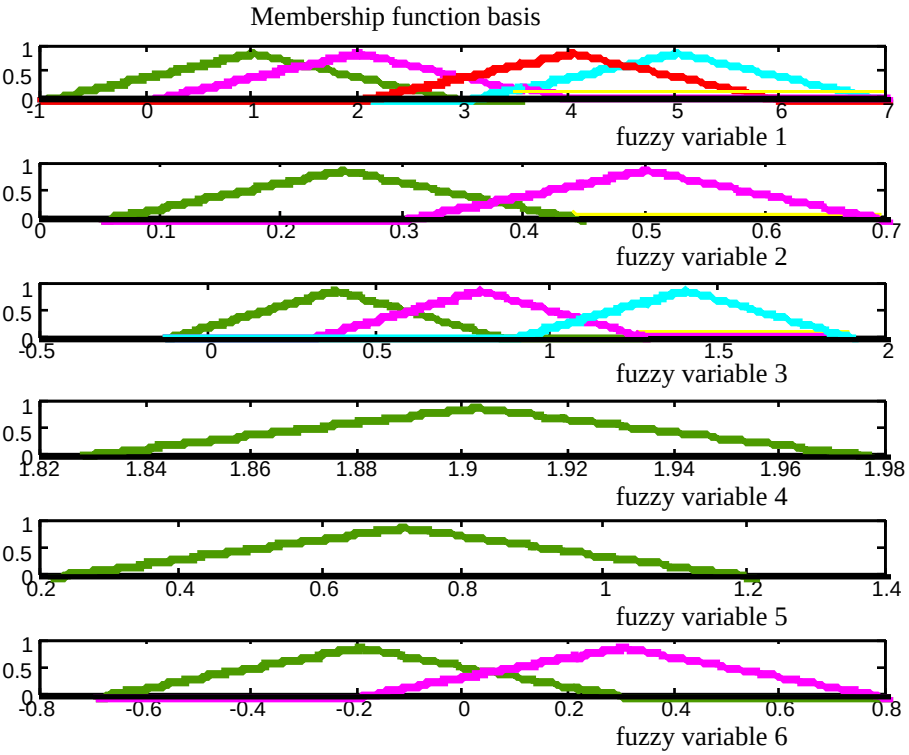

Figure 14. Membership functions created during execution of the parallel version of the training process. They correspond to the example given in section 3.5.1 and to the data summarized in Table 4.

Table 6. Learning process for the example given in Table 4. Corresponding problems and their solutions as determined automatically by our parallel implementation FUNNY-ALGORAM. mf stands for membership function and epoch for an iteration cycle.

Parameter values						Problem to be solved	Solution
mf11	mf21	mf31	mf41	mf51	mf61	START	-
mf12	mf21	mf32	mf41	mf51	mf61	2th image badly Classified! (on 1th Patient data set used)	Addition of 2 mf and 1 rule to avoid misclassification after 8 epochs
						3th Image badly Classified! (on 1th Patient data set used)	All data has been properly Classified! after 2 epochs
mf12	mf21	mf33	mf41	mf51	mf61	4th Image: no rule fired! 1 mf does not exist	Addition of 1 mfand 1 rule
mf13	mf21	mf33	mf41	mf51	mf61	5th Image: no rule fired! 1 mf does not exist	Addition of 1 mf and 1 rule
mf13	mf22	mf33	mf41	mf51	mf61	5th Image: no rule fired! 1 mf does not exist	Addition of 1 mf and 1 rule
mf14	mf21	mf33	mf41	mf51	mf62	4th Image badly Classified! (on 1th Patient data set used)	Addition of 1 mf and 1 rule to avoid misclassification after 8 epochs
mf13	mf22	mf33	mf41	mf51	mf62	5th Image badly Classified! (on 1th Patient data set used)	Addition of 1 rule to avoid misclassification after 8 epochs

Table 6 exemplifies how this modification improves the behavior of ALGORAM.

After evaluation by the trained neuro-fuzzy system, the rules corresponding to a leader which have been fired are hold back. According to the example above, the rules which have fired are the rules 1, 2 (×2), 6 and 7. The created corresponding membership functions are showed in Figure 14 in the same order.

Other methods creating automatically a rule base, such as, for example, ANFIS or the so-called subtractive algorithm, have also been implemented and tested. We believe that our implementation has several advantages with respect to these other two methods. ANFIS firstly determines all the permutations between membership functions in order to create the rules and then secondly adjusts the membership functions. This method is cumbersome and slow when we use, for example, as the input set the six parameters introduced in section 3.4.1 (see also Table 1). We have also found that the

subtractive method is not well adapted to our application, since we have to provide an output value for each input. Even if we attempt to calculate fulfillment values for the regions (or assign the value 0 to regions other than the leader, which has in fact no sense), the membership functions and rules created by these approaches are more numerous than in our approach.

4. In vitro experiments and application to medical cases

In order to validate the new approach we have implemented and to estimate its performance when applied to actual medical image data, we have carried out two types of experiments. Firstly, we have tested, adjusted and validated the whole procedure using data sets of images of phantoms modeling real acquisition conditions. Secondly, the procedure has been applied to image data acquired under medical conditions in order to assess its suitability and performance in medical routine.

4.1. Experiments with phantoms

It is difficult to assert that the myocardial volume corresponds exactly to the sum of the region areas found by our algorithm to correspond to the left ventricle in the set of acquired slices (recall that a pixel in a given slice corresponds to an elementary volume or voxel). In other words, the question is to determine to which extent the extracted contours represent actually the left ventricular cavity depicted in a slice. In addition, the ability of our algorithm to separate the two ventricular cavities, taking into account the noise, has also to be characterized. In order to evaluate both correctness and performance of our method, we have built a series of phantoms that enable to simulate the ventricular volumes. Since both shape and dimensions of our artificial "ventricles" are known, we are able to evaluate both the accuracy of the measured left ventricular volumes and the ability to separate the two ventricles, and to assess the robustness of our approach with respect to noise.

The ventricular phantom has been built with two bottles of equal diameter and volume (4.2 cm and 75 ml respectively), containing 4 mCi/cc of 99m-Tc. The distance d between the two bottles (which represents the interventricular septum) can be varied between 0 and 1.5 cm. The experimental work on this phantom has been carried out in two phases. During the first one, the diameters of the bottles have been measured as a function of the distance d. The principle of this experiment is illustrated in Figure 15. For the second phase, the bottles have been submerged in water, as shown in Figure 16, the aim being to simulate the diffusion induced by the thoracic tissues. SPECT images of our phantom have been acquired and slices have been reconstructed after backprojection using the same parameters as those used for the patient data in section 4.2.

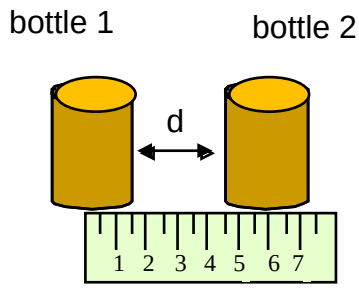

Figure 15. Principle of the first experiment carried out in order to measure the diameter of the bottles separated by a varying distance *d*.

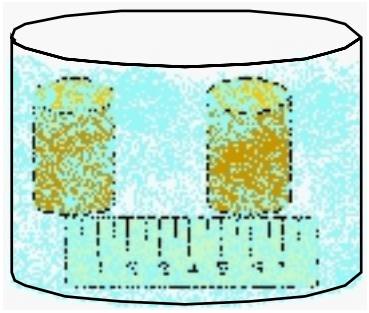

Figure 16. Principle of the second experiment carried out under conditions simulating real acquisition conditions (diffusion) in order to measure the diameter of the bottles separated by a varying distance *d*.

The three Tables 7, 8 and 9 summarize the measures obtained experimentally. The corresponding situations evaluated (test cases) are defined as follows:

case no. 1: no diffusion in the images
case no. 2: diffusion present (with water in the tank)
case no. 3: no diffusion, but with 5% of added Gaussian noise in the images
case no. 4: no diffusion, but with 15% of added Gaussian noise in the images
case no. 5: no diffusion, but with 25% of added Gaussian noise in the images

Table 7. Measured diameter for the first bottle

Real distance d between the bottles [cm]	diameter case no. 1 [cm]	diameter case no. 2 [cm]	diameter case no. 3 [cm]	diameter case no. 4 [cm]	diameter case no. 5 [cm]
0	4.5	3.9	4.5	4.5	4.5
0.2	4.5	3.9	4.2	4.2	4.9
0.5	4.5	3.9	4.5	4.5	4.2
0.7	4.8	3.9	4.2	4.9	4.5
1.0	4.8	4.2	4.9	4.9	4.2
1.5	4.5	3.9	4.5	4.5	4.5
Mean	4.62	3.96	4.47	4.58	4.47
Standard deviation	0.16	0.13	0.26	0.27	0.26

Table 8. Measured diameter for the second bottle

Real distance d between the bottles [cm]	diameter case no. 1 [cm]	diameter case no. 2 [cm]	diameter case no. 3 [cm]	diameter case no. 4 [cm]	diameter case no. 5 [cm]
0	4.2	3.3	4.2	4.2	4.5
0.2	4.2	3.3	3.9	4.2	4.5
0.5	4.2	3.6	4.2	4.2	4.2
0.7	4.2	3.2	4.2	4.2	4.2
1.0	4.5	3.6	4.5	4.5	3.9
1.5	4.5	3.6	4.5	4.5	4.2
Mean	4.32	3.48	4.25	4.3	4.3
Standard deviation	0.16	0.16	0.22	0.16	0.26

We observe that, for the five test cases investigated, our procedure recognizes the circular structure of the two bottles independently of the distance d separating them. More important, the diameters computed remain relatively constant in all the experiences, establishing that our algorithm is suitably robust with respect to the noise. In case no. 2 implying images including diffusion, the diameters found are slightly smaller. The light difference in the measured mean diameters for the two bottles can be partially related to the non-symmetrical position of the two bottles in the water tank, which modifies the diffusion of the gamma rays. Further, the influence of diffusion can also be observed in the apparent lower measured diameter when the two bottles are immersed in the water tank.

Table 9. Measured distance between the bottles (due to the small amount of data available, correlation coefficients are only indicative).

Real distance d between the bottles [cm]	measured diameter case no. 1 [cm]	measured diameter case no. 2 [cm]	measured diameter case no. 3 [cm]	measured diameter case no. 4 [cm]	measured diameter case no. 5 [cm]
0	0	0	0	0	0
0.2	0.3	0.6	0.65	0.6	0
0.5	0.6	0.6	0.65	0.6	0.6
0.7	0.6	1.0	1.0	0.6	0.6
1.0	1.0	1.3	1.0	0.6	1.6
1.5	1.3	1.9	1.3	1.31	1.6
correlation coefficient	0.98	0.97	0.92	0.87	0.84

Although the measures are correct in most of the cases, one can observe that the measured diameters are over-estimated and that accuracy decreases when the amount of noise added is too high. This is particularly critical when the distance simulating the ventricular septum is short and le level of noise high (see Table 9, case no. 5 for which

the separation between the bottles is 0.2 cm). In all the other cases, identification of the two bottles is correct when decreasing the distance between the bottles. One has also to take into account the spatial resolution of the gamma camera used, which for this series of experiments was of 0,6 mm/pixel. This value can have an impact on the results when the separation between the bottles is small. Accordingly, the correlation coefficients found for the measured distances between the bottles and given in Table 9 can be considered to be fairly good.

4. 2. Clinical Test Cases

For these experiments, we have randomly selected twelve patients and for each of them, we have routinely acquired a set of G-SPECT images. Each data set has then be processed with our procedure and the results obtained have been compared with those obtained using two other techniques routinely employed in our laboratory. The first alternative is a semi-automatic MRI technique where the contours are manually traced (MRI system GE MRMax 0.5T, sequence gradient echo TE = 12ms, TR = 39ms, FLIP=20°, Nex=2). The second one is the protocol used every day in our laboratory. For this latter method, thresholding at 40% of the maximum gray value found in the set of images enables to visualize the diastolic and systolic contours which can then be interpreted by the physician. However, an operator has to initialize image processing by selecting visually a region of interest corresponding to (including) the left ventricle and, if the two regions corresponding to the ventricles are not isolated or if some contours do not border completely the regions of interest during processing, the errors have to be manually corrected.

Table 10. Calculated LVEF values using the results of the three approaches applied.

PATIENT Number	LVEF (%) MRI based method	LVEF (%) Every day protocole	LVEF (%) Proposed method
1	53	59	55
2	59	57	53
3	68	68	42
4	59	59	67
5	58	61	48
6	77	74	62
7	55	53	48
8	53	46	54
9	67	70	51
10	7	13	1*
11	62	73	53
12	43	44	48

For the three methods, the ejection fraction has been calculated. The results are summarized in Table 10. The case marked with a star (*) corresponds to a patient with an important dilated and hypokinetic cardiomyopathy. In this case the very low value of

the LVEF obtained by the proposed method is doubtful and may correspond to a limit of the method.

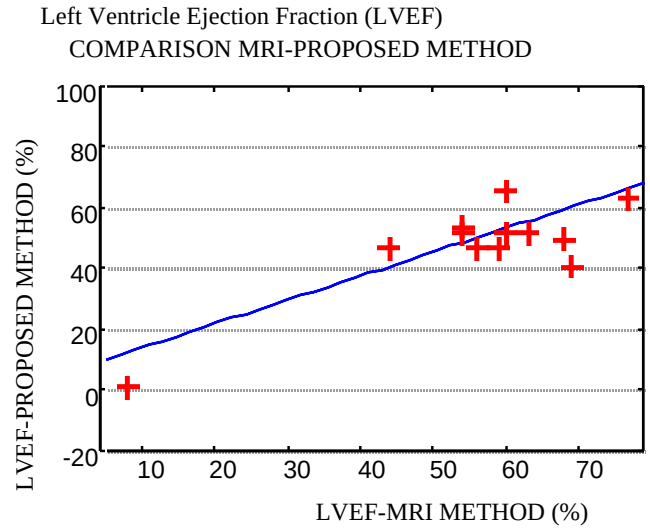

Figure 17a. Comparison of the LVEF values using the three approaches to be compared. These figures directly led to the computation of the regression coefficients *r*.

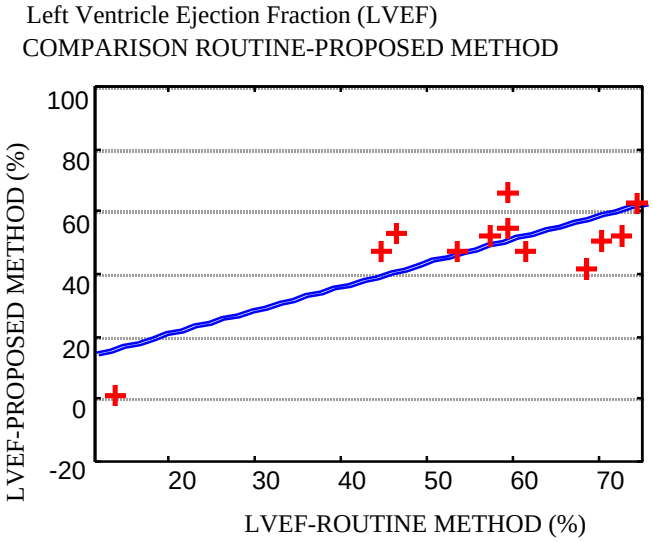

Figure 17b. Comparison of the LVEF values using the three approaches to be compared. These figures directly led to the computation of the regression coefficients *r*.

In order to assess the quality of the results achieved with our automated approach, we have calculated the regression coefficients *r* between our procedure and the other two methods (see Figure 17), as an indicative measure to be used for comparison. As a result, when comparing to the MRI based method, we have obtained r = 0.84. This coefficient takes a value of 0.78 when comparing to the routine method used in our laboratory.

Due to the limited size of the set of evaluated image data, these values for the regression coefficients r can only be considered acceptable. Also, only the data corresponding to three patients have been used to train the recognition system. It is however noteworthy that our implementation is already able to automatically select the region corresponding to the left ventricle and to extract the associated contours in order to compute the LVEF. When comparing our results with the measurements obtained with the two other techniques (MRI and standard nuclear procedure), one must remind that there is no "gold standard" method in medical imaging able to give the exact or the real value of the LVEF. That means that the correlation coefficients can only be compared in a relative way.

4. 3. Implementation issues

We have implemented our method on a Macintosh computer equipped with a 603 PowerPC processor running at 75 MHz. The algorithms have mostly been developed using the programming language of Matlab. The public domain software package Image from the NIH [24] has been used to compute the parameters related to the shape and the location of the various regions extracted from the images under investigation. The computing time for processing a whole patient data set is of the order of forty minutes. We expect however to be able to speed up execution with a new implementation using the **C or C++** programming language.

5. Conclusions

In this chapter, a new method for contouring fully automatically blood pool myocardial gated SPECT images has been presented. The method has been specifically developed in order to determine the left ventricle cavity surfaces required to be able to calculate the Left Ventricular Ejection Fraction (LVEF). The LVEF is indeed an essential diagnosis parameter in cardiology. The approach is based on the sequential application of three steps. The first step is a wavelet based image pre-processing enabling both to reduce the noise level in the images and to enhance the image contrast in order to favor separation of the regions corresponding to the two myocardial ventricles. At this stage of the processing, it is particularly crucial to find a point belonging to the border between the regions corresponding respectively to the left ventricle and the septum. This point initializes the procedure realizing the second step which performs the segmentation of the images using the neural networks leadership algorithm. This step delivers classes built with Gaussian functions, the initial first class

being centered around the border point returned by the wavelet-based processing algorithm. The third step has in charge the selection in the image of the region which corresponds to the left ventricle. This determination is made using a fuzzy logic based decision implemented as a three layer neural network. This procedure requires training in order to set up the necessary knowledge base. For that purpose, we have developed a new tool called ALGORAM, able to automatically generate rules and membership-functions. This allows to automatically create and/or enlarge both the rule and membership function bases. Combining this tool with an adaptive tuning scheme optimizes the system performance.

The proposed technique has been implemented and applied to both images of phantoms and of real patients. Results for the phantom images allow to validate our approach. Further, they show that our method is robust when applied to images corrupted with noise and is able to distinguish the two simulated myocardial ventricles. For the real patient data sets, the LVEF has been calculated and compared to a MRI based method and to the protocol used routinely in our laboratory. Even though the measures delivered by our approach are slightly underestimated with respect to the results obtained with the other two methods, the three sets of results are for all the experiments carried out in an acceptable overlapping range of values. Therefore, these results validated our method in the case of real-life image data. One can also note that the comparison is made using results from methods, which are not yet considered to be standard in this medical field. Further, even when the measures are realized by experienced operators, there are almost every time discrepancies in the results obtained by different operators evaluating the same set of images. Thus, as the results of our method approach rather well those of the other two methods and as the measures are obtained automatically, it is a good choice in order to avoid variations in the results to be used for diagnosis. This is further enhanced by the fact that the method is able to segment validly the region corresponding to the left ventricle and to extract its contour. Lastly, the recently implemented software module ALGORAM adds more autonomy to the method and makes easier enlargement of the knowledge base.

However, the current version or the implementation still lets partially open some questions related mainly to suitability of the approach in medical routine and research has to be pursued. In particular, we are currently collecting a rather exhaustive set of data corresponding to representative clinical cases using both MRI and SPECT acquisition modalities. This will enable to enlarge the knowledge base and better ground the already achieved comparison between different techniques. Also, a larger and more complete knowledge base will certainly favor the evaluation of data related to strongly pathological cases for which the data is strongly distorted. This is for example the case for some pathologies for which the systolic contours are as large as the diastolic ones. Future work will also investigate the influence of knowledge base size on performance. Indeed, if the knowledge base is too large, it could lead to confusion. Another related point is to find the optimal size, as manipulating a large rule base slows down computing speed. We believe that an extension of ALGORAM in order to "intelligently" destroy unnecessary rules could decrease execution time. Also, the number of measured parameters evaluated in the fuzzy system could be decreased to speed up the training process. This raises straightforwardly the question of the minimal number of parameters needed and of their appropriateness. For example, some of the

parameters can be replaced by one unique spatio-temporal parameter maintaining also consistency between the slices. Enhancing the segmentation step in order to have a minimum number of regions to evaluate is another interesting option. As our system is still perfectible, there remains still a lot of work to do but we find that our research takes the right way and at least in automatically contouring blood pool SPECT images we can say that the use of neuro-fuzzy techniques makes things less fuzzy.

Acknowledgements

The first author would like to thank Prof. Dr. H.-D. Kochs, Head of the Technical Computing Laboratory, and Dr. S. Baginski for their support and for the facilities made available during the development of the training method of the knowledge base at the Gerhard Mercator University, Duisburg, FRG, during a research stay partially funded by the DAAD (grant n° A/98/34202). This work is also supported by following institutions. CONACYT (Consejo Nacional de Ciencia y Tecnologia, Mexico D.F. Mexico), SFERE (Société Française d'Exportation de Ressources Educatives), Apple Computer France. The authors also would like to thank Dr. Philippe Choquet, Dr. Barbu Dumitrescu, Dr. Luc Mertz and Dr. Philippe Germain for their help and support.

ANNEXES

1. Automatic Determination of Diastolic and Systolic images

Acquisition of the images is synchronized by the R wave of the ECG (gated-SPECT image acquisition). This means that the eight phases of the cardiac cycle are acquired between two successive R waves. This operation is further repeated thirty times and enables to finally obtain a set of 240 images corresponding to 30 acquisitions. Note that the volume variation with respect to time is sampled over time (at the instants corresponding to the acquisition of the eight phases of the cardiac cycle). In other words, the specific acquisition system does not allow to derive the underlying continuous smooth function, but only an approximation thereof. The set of 240 images is then arranged into eight groups. The first group contains all the first phase images of the 30 acquisition steps, the second group the next phase images in the different acquisitions, and so on. One of these groups contains the information related to the diastolic phase and an other that of the systolic phase. These two particular groups have to be determined. Also, the sum of all the images in a given group leads to so-called accumulated radioactivity image (thus, 8 radioactivity images are obtained). Further, the sum of the intensity of all the pixels in a given radioactivity image finally gives the so-called total radioactivity coefficient for that image. The coefficient of maximal value can be shown to be related to the diastolic group and the coefficient of minimal value to the systolic group. Tomographic backprojection reconstruction is then applied to the two groups selected this way, firstly to the group corresponding to the diastolic phase, secondly to the one associated with the systolic phase.

In order to adjust the rotation centre, the diastolic image reconstructed according to the procedure above is presented to an operator in an horizontal plane and this operator manually establishes a line passing through the apex and the middle of the myocardium.

A visualization software package allows to rotate the displayed image to make coincident this line with the Horizontal Long Axis. The rotation center is then also positioned by the operator. In a second step, the lateral limits of the myocardium are established to reconstruct the Vertical Long Axis images. Further reconstruction limits regarding the apex and the base of the myocardium are established to reconstruct the Horizontal Short Axis images. These reconstruction parameters for the diastolic images are stored and automatically applied during the reconstruction of the systolic images, enabling to take care of the adjustment of the rotation centre. The reconstruction software lastly arranges routinely the whole set of diastolic and systolic images into a new group containing subsets of HSA, HLA and VLA images. Each subset contains alternatively one diastolic image followed by one systolic image. We have in this work chosen to rearrange these subsets into one diastolic and one systolic images. Also, only HSA diastolic and systolic images are used to compute the LVEF, even though HLA data could be used to ameliorate the estimate of the LVEF. However, as a result, only a slight improvement can be observed in this case.

2. Trust limits of the estimated regression coefficients

In order to complement the statistical data given in section 4. for the LVEF calculated using the three different methods, the regression coefficient between the routine method and the MRI method has been estimated to be 0.92. Calculation of the trust limits for the estimated regression coefficients are given below :

Prob(0.51<r<0.954) = 0.95 for MRI method-Proposed method
Prob(0.37<r<0.935) = 0.95 for Routine method-Proposed method
Prob(0.73<r<0.976) = 0.95 for Routine method-MRI method

There is indeed a better agreement between the Routine method and the MRI method but, as stated in section 4, there is no standard method available. One can thus not expect that our results exactly approach those of the other methods. However, it is acknowledged that training of the system with an enlarged set of patient data would surely improve the quality of the results and enable to deal with situations where operator based contouring decisions could lead to inconsistencies.

It must also be mentioned that no correction factor has been applied to the LVEF calculation, even if it is known that there is a systematic underestimation of the volumes in the presence of diffusion. This can be seen clearly when studying the phantom of the left ventricle. However, in the case or real heart data, this error is difficult to estimate as no accurate model is available. Further, the estimation error is systematic and thus leads to underestimate volumes. As a result, the LVEF being a ratio of volumes smaller than 1, this quantity is slightly underestimated. Note however that there is a partial compensation of the error, the underestimation affecting both terms of the ratio. Applying a correction factor for the diastolic and systolic volumes thus only slightly ameliorates the LVEF values.

BIBLIOGRAPHY

1. **Zadeh, L.,** Fuzzy sets, *Information and Control*, 8, 338-356, 1965.

2. **Boegl, K. *et al.*,** New approaches to computer-assisted diagnosis of rheumatologic diseases, *Radiologe*, 35 (9), 604-610, 1995.
3. **Pietka, E.,** Computer-assisted bone age assessment based on features automatically extracted from a hand radiograph, *Comput. Med. Imaging Graph*, 19 (3), 251-259, 1995.
4. **Shiomi, S., *et al.*,** Diagnosis of chronic liver disease from liver scintiscans by fuzzy reasoning, *J. Nucl. Med*, 36 (4), 593-598, 1995.
5. **Phillips, W., *et al.*,** Automatic magnetic resonance tissue characterization for three-dimensional magnetic resonance imaging of the brain, *J. Neuroimaging*, 5 (3), 171-177, 1995.
6. **Phillips, W., *et al.*,** Application of fuzzy c-means segmentation technique for tissue differentiation in MR images of a hemorrhagic glioblastoma multiforme, *Magn. Reson. Imaging*, 13 (2), 277-290, 1995.
7. **Brandt, M., *et al.*,** Estimation of CSF, white and gray matter volumes in hydrocephalic children using fuzzy clustering of MR images, *Comput. Med. Imaging Graph*, 18 (1), 25-34, 1994.
8. **Bezdek, J., *et al.*,** Medical image analysis with fuzzy models, *Stat. Methods Med. Res.*, 6 (3), 191-214, 1997.
9. **Lippmann, R.,** An introduction to computing with neural nets, *IEEE ASSP mag*, 4, 4-22, 1987.
10. **Lin, J.-S., *et al.*,** Application of artificial neural networks for reduction of false-positive detections in digital chest radiographs, *Proc. Annu. Symp. Compt. Appl. Med. Care*, 434-438, 1993.
11. **Lin, J.-S., *et al.*,** Segmentation of multispectral magnetic resonance image using penalized fuzzy competitive learning network, *Compt. Biomed. Res.*, 29 (4), 314-326, 1996.
12. **Germano, G., *et al.*,** Automatic quantification of ejection fraction from gated myocardial perfussion SPECT, *J. Nucl. Med.*, 36, 2138-2147, 1995.
13. **Chin, B. B., *et al.*,** Right and left ventricular volume and ejection fraction by tomographic gated blood-pool scintigraphy, *J. Nucl. Med*, 38, 942-948, 1997.
14. **Meyer, Y.,** Les ondelettes: algorithmes et applications, Armand Colin, Paris, France, 1994.
15. **Strang, G., Nguyen T.,** Wavelets and filter banks, Wellesley-Cambridge Press, Wellesley Ma., USA, 1996.
16. **Carpenter, G. A., Grossberg, S.,** A massively parallel architecture for a self-organizing neural pattern recognition machine, *Computer vision, graphics and image processing*, 37, 54-115, 1987.
17. **Carpenter, G. A., Grossberg, S.,** The ART of adaptive pattern recognition by a self-organizing neural network, *Computer*, 21 (3), 77-88, 1988.
18. **Kaparthi, S., Nallan, C. S., Cerveny, R. P.,** An improved neural network leader algorithm for part-machine grouping in group technology, *European Journal of Operational Research*, 69, 342-356, 1993.
19. **Mallat, S., Zhong, S.,** Characterization of signals from multiscale edges, *IEEE Trans. PAMI*, 11, 710-732, 1992.
20. **Mallat, S., Hwang, L.,** Singularity detection and processing with wavelets. *IEEE Trans. PAMI*, 14, 617-643, 1992.

21. **Mallat, S.,** A theory for multiresolition signal decomposition: the wavelet representation, *IEEE Trans. PAMI*, 11, 674-693, 1989.
22. **Hajj, H., Nguyen, T., Chin, R.,** On multiscale feature detection using filter banks, *Proceedings of the Asilomar Conference on Signals, Systems and Computers*, 29, 1996.
23. **Bensaid, A. M., Bezdek, J. C.,** Partial Supervision based on point-prototype clustering algorithms, *Proceedings of EUFIT '96*, 2, 1402-1406, 1996.
24. **Rasband W.,** NIH Image Public Domain Program. *U. S. National Institutes of Health, http:/rsb.info.nih.gov/nih-image/*, 1997.
25. **Patino, L., Mertz, L., Hirsch, E., Dumitrescu, B., Constantinesco, A.,** Contouring blood pool myocardial gated SPECT images with a neural network leader segmentation and a decision-based fuzzy logic, *Proceedings of FUZZ IEEE '97*, Barcelona, Spain, 2, 969-974, 1997.
26. **Patino, L., Mertz, L., Hirsch, E., Constantinesco, A.,** Segmentation and contouring of blood pool myocardial SPECT images with wavelet-fuzzy constraints, *Proceedings of EUFIT '96,* Aachen, Germany, 3, 2086-2090, 1996.
27. **Bersini, H., Gorrini, V.,** FUNNY (FUzzY or Neural Net) methods for adaptive process control, *Proceedings of EUFIT '93*, 2, 55-61, 1993.
28. **Berenji, H. R., Khedkar, P.,** Learning and tuning fuzzy logic controllers through reinforcements, *IEEE Trans. neural networks*, 3, 724-740, 1992.
29. **Berenji, H. R., *et al*.,** Space shuttle attitude control by reinforcement learning and fuzzy logic, *Proceedings of IEEE Int. Conf. on Neural Networks*, 1396-1401, 1993.
30. **Nomura, H., Hayashi, I., Wakami, N.;** A learning method of fuzzy Inference rules by descent method, *Proceedings of IEEE Int. Conf. on Fuzzy Systems*, 203-210, 1992.
31. **Jang, J.-S.,** ANFIS: Adaptive neuro fuzzy inference systems, *IEEE Trans. Systems, Man & Cybernetics*, 23, 665-685, 1993.
32. **Sulzberger, S. M., *et al*.,** FUN: Optimization of fuzzy rule based systems using neural networks, *Proceedings of IEEE Int. Conf. on neural networks*, 312-316, 1993.
33. **Nauck, D., Kruse, R.,** A fuzzy neural network learning fuzzy control rules and membership functions by fuzzy error backpropagation, *Proceedings of IEEE Int. conf. on neural networks*, 1022-1027, 1993.
34. **Nauck, D., Klawonn, F., Kruse, R.,** Das NEFCON Modell, in *Neuronale netze und fuzzy-systeme*, Vieweg, Braunschweig, Germany, chap. 19, 1996.
35 **Jang, J.-S., Sun, C.-T., Mizutani, E.,** Neuro-Fuzzy and Soft Computing, Eds., Prentice Hall, New Jersey, USA, 1997.
35b. **Jang, J.-S.,** Equivalent ANFIS architecture, in Neuro-Fuzzy and Soft Computing, Eds., Prentice Hall, New Jersey, USA, chap. 12, 1997.
36 **Baginski, S.,** personal communication, *Technische Informatik, Gerhard Mercator Universität, Duisburg, FRG, http://mti.uni-duisburg.de/~baginski/*, 1998.

ACRONYMS

ALGORAM	**A**utomatic **L**eader **G**eneration **O**f **R**ules **A**nd **M**embership functions
ART	**A**daptive **R**esonance **T**heory
ANFIS	**A**daptive **N**euro-**F**uzzy **I**nference **S**ystem
G-SPECT	**G**ated - **S**ingle **P**hoton **E**mission **C**omputed **T**omography
FUNNY	**FU**zz**Y** and **N**eural **N**etworks
HSA	**H**orizontal **S**hort **A**xis
HLA	**H**orizontal **L**ong **A**xis
VLA	**V**ertical **L**ong **A**xis
LVEF	**L**eft **V**entricle **E**jection **F**raction
SPECT	**S**ingle **P**hoton **E**mission **C**omputed **T**omography